HHS Public Access

Author manuscript

Cell. Author manuscript; available in PMC 2020 April 04.

Published in final edited form as:

Cell. 2019 April 04; 177(2): 256–271.e22. doi:10.1016/j.cell.2019.02.014.

Multi-sensory gamma stimulation ameliorates Alzheimer's-associated pathology and improves cognition.

Anthony J. Martorell[1,2,#], **Abigail L. Paulson**[3,#], **Ho-Jun Suk**[4,5,6,*], **Fatema Abdurrob**[1,2,*], **Gabi Drummond**[1,2], **Webster Guan**[7], **Jennie Z. Young**[1,2], **David Nam-Woo Kim**[1,2], **Oleg Kritskiy**[1,2], **Scarlett Barker**[1,2], **Vamsi Mangena**[6], **Stephanie M. Prince**[3], **Emery N. Brown**[1,2,8,10,11], **Kwanghun Chung**[1,2,7,8], **Edward S. Boyden**[2,4,5], **Annabelle C. Singer**[3], **Li-Huei Tsai**[1,2,9,12]

[1]Picower Institute for Learning and Memory, Massachusetts Institute of Technology, Cambridge, Massachusetts 02139, USA.

[2]Department of Brain and Cognitive Sciences, Massachusetts Institute of Technology, Cambridge, Massachusetts 02139, USA.

[3]Coulter Department of Biomedical Engineering, Georgia Institute of Technology and Emory University School of Medicine, Atlanta 30332 USA

[4]McGovern Institute for Brain Research, Massachusetts Institute of Technology, Cambridge, Massachusetts 02139, USA.

[5]MIT Media Lab, Departments of Biological Engineering and Brain and Cognitive Sciences, Massachusetts Institute of Technology, Cambridge, Massachusetts 02139, USA.

[6]Harvard-MIT Health Sciences and Technology, Cambridge, Massachusetts 02139, USA.

[7]Department of Chemical Engineering, MIT, Cambridge, Massachusetts, USA

[8]Institute for Medical Engineering and Science, Massachusetts Institute of Technology (MIT), Cambridge, Massachusetts, USA.

[9]Broad Institute of Harvard and MIT, Cambridge, Massachusetts 02139, USA.

Corresponding author: Li-Huei Tsai, Picower Institute for Learning and Memory, Massachusetts Institute of Technology, Cambridge, Massachusetts 02139, lhtsai@mit.edu, phone: 617-324-1660, fax: 617-324-1657, web: http://tsailaboratory.mit.edu.

[#]Senior author

[*]These authors contributed equally

Contributions

A.J.M., A.C.S., A.L.P., J.Z.Y, E.N.B., E.S.B., K.C., and L.-H.T. designed experiments. A.C.S. and A.L.P. performed and analyzed electrophysiology data. S.M.P assisted with electrophysiology experiments. A.J.M. and D.N-W.K. performed and analyzed ELISA experiments. O.K. performed western blots. A.J.M. performed behavior experiments. D.N-W.K. analyzed behavior experiments. A.J.M., D.N-W.K., and F.A. performed and analyzed imaging experiments. F.A. performed and analyzed 3D microglia clustering quantification. G.D., W.G., and V.M. performed and analyzed whole brain SHIELD experiments. A.J.M., D.N-W.K., and F.A. performed auditory and combined GENUS experiments. H-J.S. and A.C.S. engineered auditory and combined GENUS sounds and equipment. A.J.M., A.C.S, A.L.P, J.Z.Y. and L.-H.T. wrote the manuscript. All authors read and revised the manuscript.

Conflict of Interest

L.-H.T. and E.S.B are co-Scientific Founders and serve on the scientific advisory board of Cognito Therapeutics and A.C.S. owns shares of Cognito Therapeutics Inc.

[10]Department of Anesthesia, Critical Care, and Pain Medicine, Massachusetts General Hospital, Boston, MA, 02114

[11]Harvard Medical School, Boston, MA 02115

[12]Lead contact

Summary

We previously reported that inducing gamma oscillations with a non-invasive light flicker (Gamma ENtrainment Using Sensory stimulus, or GENUS) impacted pathology in the visual cortex of Alzheimer's disease mouse models. Here, we designed auditory tone stimulation that drove gamma frequency neural activity in auditory cortex (AC) and hippocampal CA1. Seven days of auditory GENUS improved spatial and recognition memory and reduced amyloid in AC and hippocampus of 5XFAD mice. Changes in activation responses were evident in microglia, astrocytes, and vasculature. Auditory GENUS also reduced phosphorylated tau in the P301S tauopathy model. Furthermore, combined auditory and visual GENUS, but not either alone, entrained gamma oscillations, produced microglial-clustering responses, and decreased amyloid in medial prefrontal cortex. Whole brain analysis using SHIELD revealed widespread reduction of amyloid plaques throughout neocortex after multi-sensory GENUS. Thus, GENUS can be achieved through multiple sensory modalities with wide-ranging effects across multiple brain areas to improve cognitive function.

Graphical Abstract

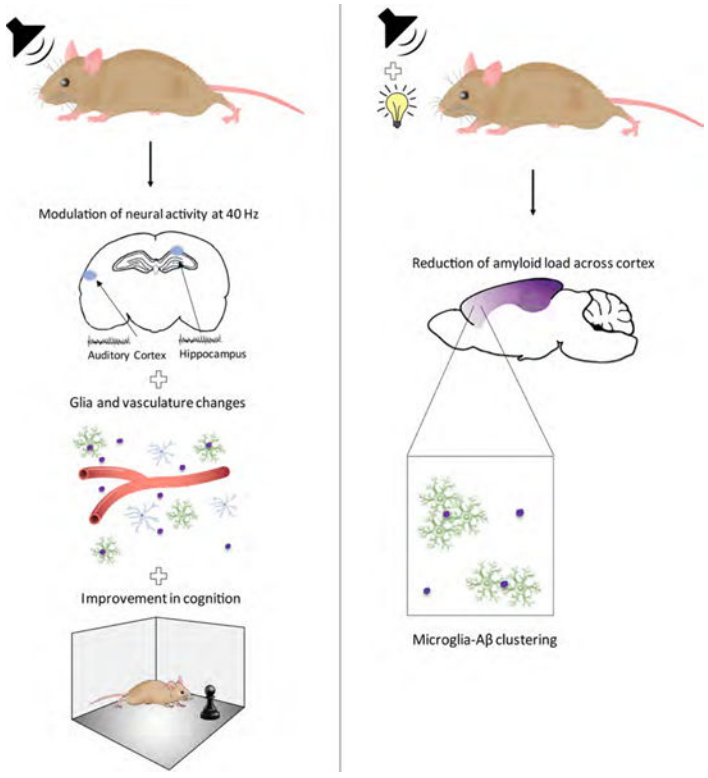

Keywords

Alzheimer disease; gamma rhythms; acoustic stimulation; photic stimulation; amyloid; microglia; astrocytes; vasculature; memory; cognition

Introduction

Alzheimer's disease (AD) is the most prevalent form of dementia and is characterized by the progressive loss of cognition, for which there are currently limited treatment options. Pathological hallmarks of the disease include extracellular aggregates of amyloid-β (Aβ) peptides and tau-associated pathology (Hardy and Higgins, 1992, Selkoe et al., 1996, Yankner and Lu, 2009, Verret et al., 2012). Aberrant neural activity can also exacerbate the progression of AD-pathology, which ultimately disrupt neural circuits involved in higher cognitive functions (Palop et al., 2007, Canter et al., 2016). Conversely, neural activity can also be modulated to reduce AD pathology (Cirrito et al., 2005, Bero et al., 2011, Iaccarino et al., 2016), but whether it can improve cognitive function in AD remains to be determined.

For instance, gamma oscillations (30–90 Hz), associated with numerous higher-order cognitive functions (Fries, 2009), are disrupted in several AD mouse models (Verret et al., 2012, Gillespie et al., 2016, Iaccarino et al., 2016). We and others have shown that gamma oscillations can be evoked with optogenetics (Cardin et al., 2009, Sohal et al., 2009) or non-invasively, which we term Gamma ENtrainment Using Sensory stimuli (GENUS), via a light programmed to flicker at 40 Hz (Rager and Singer, 1998, Iaccarino et al., 2016). In our previous study (Iaccarino et al., 2016), we used visual GENUS to entrain gamma oscillations in the primary visual cortex (VC), and found a reduction in amyloid load and morphological changes in microglia - such as enlarged soma size and increased co-localization with Aβ - consistent with a more phagocytic state (Saijo and Glass, 2011, Walker and Lue, 2015). These findings showed that visual GENUS can affect local network activity and induce a protective molecular and cellular response in VC of 5XFAD mice. However, AD affects multiple brain centers critical for learning and memory, and other higher-order brain functions, such as the hippocampus (HPC) and medial prefrontal cortex (mPFC) (Seeley et al., 2009, Sperling et al., 2010, Yamamoto et al., 2014, Spellman et al., 2015, Kim et al., 2016). Thus, some outstanding questions in the application of GENUS include: can GENUS 1) be induced through other sensory modalities to reduce AD pathology? 2) have impact beyond primary sensory areas? 3) improve cognitive function in AD? 4) be achieved through multi-sensory stimuli to further impact downstream brain regions?

Here, we tested the application of GENUS using auditory stimulation with a train of tones flickering at 40 Hz. We show that auditory GENUS significantly improved performance on several hippocampal-dependent tasks. Concurrently, we observed reduced amyloid load and microglial responses consistent with increased phagocytosis in the auditory cortex (AC) and HPC of 5XFAD mice. Auditory GENUS also increased the number of reactive astrocytes and elicited a vasculature response in these brain regions. Finally, we found that combined auditory and visual GENUS uniquely induced a microglia-clustering response in AC, HPC, as well as mPFC, and reduced amyloid load not just in these brain regions but throughout

the neocortex. Our observations demonstrate a non-invasive approach to elicit system-wide effects on AD-related pathology and improvements in cognition in an AD mouse model.

Results

40 Hz auditory stimulation modulates spiking activity in AC, CA1, and mPFC

We first determined whether auditory tone stimulation could produce GENUS in AC, area CA1 of HPC, and mPFC. We presented animals with trains of tones repeating at 20 Hz, 40 Hz, 80 Hz, or with trains of randomly spaced tones (1 ms-long, 10 kHz tones played every 12.5 ms, 25 ms, 50 ms, or with random inter-tone intervals, henceforward referred to as "auditory stimulation", Methods). We recorded neural activity in AC, CA1, or mPFC during tone presentation using 32 channel silicon probes in 3–8 month old male wild-type (C57BL6J) mice as they ran or rested on a spherical treadmill. The firing rate of putative single units increased and decreased periodically with each tone thereby entraining to the 40 Hz auditory stimulation (Figure 1A, G, and M; Figure 1B, H, and N, blue). Units were also modulated by random stimulation: when all random pulses were aligned, there was a change in firing rate modulation following the stimuli, indicating that single units responded to the random stimuli pulses. However, the random train of auditory tones did not induce periodic firing modulation because the stimuli themselves were not periodic (Figure 1B, H, and N, orange). Entrainment to auditory stimulation varied between single units in both phase distribution and amplitude. During auditory stimulation, neurons fired as a function of the stimulus, but did not fire on every cycle and often at a wide range of phases: in response to 40 Hz auditory stimulation most neurons fired every 0–22 pulses in AC, 0–30 pulses in CA1, and 0–34 pulses in mPFC (1^{st} – 3^{rd} quartiles reported; Figure 1B, H, and N; Figure 1E, K, and Q), although the interval between peaks in firing rate was around 25 ms (equivalent to 40 Hz) in the majority of single units (Figure 1C, I, and O). In contrast, during baseline periods with no tones and periods with random tones, the interval between peaks had a broad distribution around 25 ms (i.e. the firing rate was not modulated at 40 Hz; Figure 1C, I, and O). Modulation strength was quantified by considering single unit firing rate as a function of the stimulus phase and calculating its vector strength (VS) (Figure 1D, J, and P, *left*). Vector strength values range from 0 to 1: 0 represents a uniform distribution of firing not modulated by the stimulus (VS = 0) and 1 represents a distribution where a neuron only fired to a specific stimulus phase (VS = 1). The distribution of vector strengths of single-unit response to 40 Hz auditory stimulation was significantly higher than no stimulation and random stimulation (Figure 1D, J, and P, *center*). Random stimulation vector strengths were also significantly higher than no stimulation (because vector strength measures modulation by a stimulus), but it did not induce periodic firing modulation. Similarly, the distribution of Rayleigh statistics for single units during 40 Hz auditory stimulation was significantly higher than that of no stimulation and random stimulation controls (Figure 1D, J and P, *right*). Differences in vector strength and Rayleigh statistics between stimulation conditions within single units showed that neurons were more strongly modulated by periodic stimuli, and that single units were significantly more strongly modulated by lower frequencies of stimulation (Figure S1G, N, and U). The mean firing rate of single neurons was similar between 40 Hz auditory stimulation and no stimulation, random stimulation, 20 Hz, and 80 Hz auditory stimulation controls (Figure 1F, L, and R; Figure S1D, K, and R). Local field

potentials in AC displayed elevated power at 40 Hz during 40 Hz auditory stimulation, but the effects varied between recording locations, recording sessions, and response latency to mapping tones (Figure S1B, I, and P). These findings suggest that 40 Hz auditory stimulation induces GENUS robustly in AC, CA1, and mPFC.

Auditory GENUS improves memory performance in 5XFAD mice

Given that auditory GENUS influences hippocampal neural activity, we next assessed its effects on hippocampus-dependent learning and memory in 6-month-old 5XFAD mice (Figure 2A), the age at which behavioral impairments first become evident (Oakley et al., 2006). Mice were first habituated to the behavior chamber 24 hrs prior to running novel object recognition (NOR) and novel object location (NOL) tasks, which test memory for the identity or placement of an object in a specific context as measured by the recognition index (Methods) (Leger et al., 2013). During habituation, neither auditory GENUS nor random frequency groups differed significantly from no stimulation controls in average velocity, total distance, time spent in the center, and time spent in the periphery, indicating no differences in general activity or anxiety-like behavior (Figure S2E–H). Following auditory GENUS, 5XFAD mice exhibited a significantly higher recognition index in NOR (65.50 ± 1.40%) and NOL (61.41 ± 2.0%) tasks, whereas no stimulation and random frequency controls had a recognition index around chance on both tasks (Figure 2B and E) - i.e., mice following auditory GENUS spent significantly more time with the novel object in NOR (Figure S2A) or object in a novel location in NOL, whereas no stimulation or random frequency controls showed no preference in either tasks (Figure S2C). Multiple comparisons (Kruskal-Wallis test with Dunn's multiple comparison test) between all frequency groups in this article are shown in Supplement Table 1. Auditory GENUS and random frequency groups did not differ significantly in distance traveled nor average velocity during the task periods versus no stimulation controls, indicating that higher recognition index is not due to general differences in activity (Figures 2C, D, F, and G). We also observed no significant difference in the time it took to reach the object exploration requirement of 20 s between auditory GENUS and random frequency groups versus no stimulation controls (Figure S2B and D).

We next applied the Morris water maze (MWM) to test spatial memory for the location of a hidden platform with respect to surrounding contextual cues (Morris, 1984, Vorhees and Williams, 2006). All three groups identified the hidden platform over successive training trials (Methods), although the escape latency for the auditory GENUS group was consistently and significantly shorter than both no stimulation and random frequency control groups (Figure 2H). There was no significant difference in swim velocity between auditory GENUS and random frequency groups versus no stimulation controls (Figure S2I). During the probe trial (Methods) mice that received auditory GENUS, but not random frequency, spent a significantly longer time exploring the quadrant that previously contained the platform and had a higher number of crossings over the platform location, versus no stimulation controls (Figure 2I and J). We additionally examined the activity of 5XFAD mice during exposure to 1 hr auditory GENUS, random frequency, or no stimulation. We observed no significant differences in average velocity (cm/s), distance traveled (cm), nor periods of quiescence (the amount of time mice spent under 2 cm/s) during the 1 hr of

GENUS or random stimulation versus no stimulation controls (Figure S2J–L). We also performed NOR, NOL, and MWM tests on 12-week old C57Bl/6J mice following 7 days of auditory GENUS, random frequency, or no stimulation. In both NOR and NOL tests, we found no significant difference in recognition index between auditory GENUS and random frequency groups versus no stimulation controls. In MWM, we observed no significant difference in the training curves nor probe tests between auditory GENUS and random frequency versus no stimulation controls (data not shown). Together, these results show that auditory GENUS can improve recognition and spatial memory in 6-month-old 5XFAD mice.

Auditory GENUS reduces amyloid load in AC and hippocampus in 5XFAD mice

The effects of auditory GENUS on hippocampal function led us to investigate if amyloid pathology could be affected in HPC. We observed that soluble $A\beta_{1–42}$ and $A\beta_{1–40}$ levels were reduced in AC ($A\beta_{1–42}$: 51.84±4.98%, $A\beta_{1–40}$: 20.65 ±3.21%) and HPC ($A\beta_{1–42}$: 46.89 ±3.89%, $A\beta_{1–40}$: 34.15 ± 4.83%) after 7 days of auditory GENUS, but not in other frequency groups, versus no stimulation controls (Figure 3A and Figure S3A), and insoluble $A\beta_{1–42}$ levels were similarly reduced in AC (36.68 ±3.21%) and HPC (43.84 ±2.42%) (Figure 3B). Insoluble $A\beta_{1–40}$ was not detectable via ELISA in auditory GENUS nor in no stimulation controls. Amyloid reduction was specific to 40 Hz stimulation, as neither 8 Hz, 80Hz, nor random frequency stimulation significantly changed Aβ levels, versus no stimulation controls. We also examined Aβ levels after 7 days of auditory GENUS in another AD mouse model using 6-month-old APP/PS1 mice, and found significantly reduced soluble $A\beta_{1–42}$ in AC (48.39±3.50%) and in HPC (35.54±4.27%), versus no stimulation controls (Figure S3B).

We next examined plaque load in 6-month-old 5XFAD mice after auditory GENUS versus no stimulation controls. Immunostaining with a β-amyloid specific antibody D54D2 (Figure 3C and D) revealed significantly reduced plaque numbers (AC: 45.73±2.818%; CA1: 59.30±2.083%) (Figure 3E) and size (AC: 54.37±5.603%; CA1: 40.70±5.321%) (Figure 3F) after auditory GENUS. Immunostaining with the $A\beta_{1–42}$-specific antibody 12F4 also showed significant reductions (AC: 45.35±0.011%; CA1: 43.21±0.0285%) (Figure 3G–I). We carried out similar analysis in another AD model, 9-month-old APP/PS1 mice (6-month-old APP/PS1 mice do not have significant plaque load). Consistent with our findings in 5XFAD mice, we saw significantly reduced plaque numbers (AC: 52.65 ± 7.53%; CA1: 62.90 ± 15.5%) and size (AC: 67.90 ± 6.18%; CA1: 64.06 ± 15.2%) after auditory GENUS. Immunostaining for $A\beta_{1–42}$ (12F4) also showed significant reductions (AC: 38.77 ± 4.21%; CA1: 47.63 ± 6.08%) (Figure S3C–E). To examine the dynamics of plaque load after auditory GENUS, we analyzed β-amyloid (D54D2) immunostaining in 6-month-old 5XFAD mice one week (with no stimulation) after 7 days of auditory GENUS concluded. We observed slight, non-significant decreases in average plaque number, size, and amyloid intensity, one week after auditory GENUS versus no stimulation controls (Figure S3F–H).

Collectively, these results demonstrate that auditory GENUS can reduce amyloid load in areas outside of primary sensory cortices in multiple AD mouse models.

Auditory GENUS induces a glia and blood vessel response in 5XFAD mice

Accumulating evidence suggests that microglia are responsive to changes in neuronal activity, and play a role in AD pathology (Allen and Barres, 2005, Mosher and Wyss-Coray, 2014, Walker and Lue, 2015). We previously observed morphological changes in microglia in 3-month-old 5XFAD after 1 hr of visual GENUS (Iaccarino et al., 2016). We thus immunostained for the microglia marker Iba1 in AC and CA1 of 6-month-old 5XFAD mice after auditory GENUS and compared to no stimulation controls (Figure 4A and B). We observed around 60% more microglia in both AC and CA1 after auditory GENUS (Figure 4C). Microglia cell body diameter was increased in both areas (AC: 70.60±4.78%; CA1: 117.17±10.4%) (Figure 4D) and additionally, microglia process length decreased (AC: 46.44±3.2%; CA1: 50.875.±4.8%) and arborization increased (AC: 36.00±9.5%; CA1: 143.813±29.9%) after auditory GENUS (Figure 4E and F). We co-immunostained for $A\beta_{1-42}$ (12F4) with microglia (Iba1) to evaluate microglia uptake of Aβ and observed an increased percentage of co-labeled microglia in AC (58.75±1.25%) and CA1 (61.33±3.71%) after auditory GENUS (Figure 4G). We also examined microglia morphology after auditory GENUS in another AD mouse model, 9-month old APP/PS1 mice. Consistent with our findings in 5XFAD mice, we observed a significant increase in microglia numbers and cell body diameter, with a significant decrease in average processes length in AC and CA1 after auditory GENUS, compared to no stimulation controls (Figure S4A–C). To examine the longitudinal effects of auditory GENUS on microglia morphology, we analyzed Iba1 immunostaining in 6-month-old 5XFAD mice one week (with no stimulation) after 7 days of auditory GENUS concluded. We observed no significant change in microglia number, cell body diameter, nor average processes length in AC one week after auditory GENUS, versus no stimulation controls (Figure S4D–F). We did, however, see a significant increase in microglia count in CA1 (41.70 ± 6.75%) in the auditory GENUS group (Figure S4F).

Astrocytes are another primary glial cell in the central nervous system, and are critical for many important biological processes including waste clearance (Chung et al., 2015, Kisler et al., 2017). We first determined that 5XFAD mice have significantly fewer reactive-like astrocytes that immunostain positive for glial fibrillary acidic protein (GFAP) than WT controls (Figure S4G and H), consistent with reports of glia atrophy in other AD mouse models (Rodríguez et al., 2009). We then immunostained for GFAP after auditory GENUS and found increased numbers in AC (GFAP: 27.66±0.954%) and CA1 (18.14±0.799%), versus no stimulation controls (Figure 4H and J). We confirmed the effects of auditory GENUS on reactive-like astrocytes using a second marker, S100 calcium-binding protein B (S100B) (AC: 21.83±1.07%; CA1: 15.57±0.869%) (Figure 4I and K). Astrocytes are also capable of regulating the brain's vascular network (Kyrtsos and Baras, 2015), which can play a role in amyloid clearance from the brain (Kyrtsos and Baras, 2015, Storck et al., 2016, Iliff et al., 2012). We first immunostained for tomato lectin, a marker of vascular endothelium, to assess vasodilation (Figure 5A and B) and observed increased blood vessel diameter after auditory GENUS (AC: 49.70 ±7.80%; CA1: 104.70 ±10.96%), versus no stimulation controls (Figure 5C). Amyloid transcytosis through the brain endothelium is mediated by lipoprotein receptor-related protein 1 (LRP1) (Kanekiyo et al., 2013, Storck et al., 2016). We thus examined co-immunostained for Aβ with LRP1 (Figure 5D and E) and observed increased co-localization of the two after auditory GENUS (AC: 53.87±2.70%;

CA1: 57.78±1.73%) (Figure 5F). Together, these results suggest auditory GENUS may elicit increased clearance of Aβ through microglia and changes in the vasculature.

Auditory GENUS reduces tau phosphorylation and seeding in AC and hippocampus

Tau phosphorylation at specific amino acid residues is a classical AD hallmark, and we previously showed that visual GENUS reduced tau hyperphosphorylation in another AD-associated mouse model, Tau P301S mice (Yoshiyama et al., 2007). We similarly investigated the effects of auditory GENUS by immunostaining (Figure S5A,B,D, and E) and saw reduced tau phosphorylation at threonine-181 (T181) (AC: 36.20±2.828%; CA1: 38.70±2.737%) and serine-396 (S396) (AC: 37.90±3.469%; CA1: 40.80±4.528%), versus no stimulation controls (Figure S5C and F). Tau phosphorylation at S396 was confirmed by Western Blot (WB) (AC: 33.83±0.20%; whole HPC: 43.20±1.50%) (Figure S5G,H,J, and K). WB analysis confirmed reduction in tau T181 phosphorylation in HPC (34.50±1.61%), although the difference was not significant in AC (AC data not shown) (Figure S5I and L). We performed a tau seeding assay to investigate effects of auditory GENUS on proteopathic tau propagation, and observed significantly decreased average change in FRET signal (Methods) (Holmes et al., 2014) in AC (72.5 ± 9.2%) and HPC (77.5 ± 5.6%) (Figure S5M). Overall, our results show that auditory GENUS can reduce the levels of hyperphosphorylated tau epitopes and seeding in a tauopathy mouse model.

Combined auditory and visual GENUS induces a clustering phenotype response by microglia

Having shown that GENUS can be applied through both visual (Iaccarino et al., 2016) and auditory stimulation, we next aimed to investigate if a combination of 40 Hz auditory tone stimulation with 40 Hz light flicker (combined GENUS) could entrain neural responses in AC, CA1, and mPFC and possibly have stronger effects than either sensory modality alone. We presented 3–8 month old male wild-type (C57BL6J) mice with 1 ms-long auditory tones coupled with 12.5 ms-long light pulses (auditory plus visual, or A+V, stimulation) at 40 Hz while recording neural activity in AC, CA1, or mPFC using 32-channel silicon probes as animals ran or rested on a spherical treadmill (Methods). Single unit firing rate increased and decreased periodically with each tone and light-on period, thus entraining to 40 Hz during combined GENUS (Figure 6A–C, *left*). Across AC, CA1, and mPFC, vector strength distributions were significantly higher, illustrating entrained spiking of single neurons to 40 Hz A+V, compared to random and no stimulation periods (Figure 6A–C, *right*). We observed elevated power in the LFP at 40 Hz in AC, CA1, and mPFC during 40 Hz A+V stimulation (Figure S6A, H, and O). Although the increase in LFP power was very small in mPFC, the median distribution of mean firing rate differences during A+V stimulation, compared to no stimulation, differed significantly from zero (Figure S6O, R) whereas neither effects were seen in mPFC with auditory GENUS alone (Figure S1P, R). Thus, combined tone plus light stimulation at 40 Hz induced GENUS in AC, CA1, and mPFC. Significant entrainment was also observed in all three regions with 20 Hz, 80 Hz, and random frequency A+V stimulation, although the latter did not induce periodic firing modulation (Figure S6B–G, I–N, P–U).

We next examined the morphological features of microglia and their interactions with Aβ in AC, VC, CA1, and mPFC in response to combined (A+V) GENUS (Figure 6D and E). Microglia exhibited a significant increase in number and soma area while projection length significantly decreased following combined GENUS versus no stimulation controls (Figure 6F–H). With auditory or visual GENUS alone, microglia displayed enlarged soma area with reduced projection length and increased in number in AC, VC, and CA1, but not in mPFC (Figure S7A–E, G–I). Additionally, we observed a unique encapsulating effect by microglia around amyloid deposits after combined GENUS. We applied IMARIS to quantify the number of microglia within a 25 μm radius of an amyloid deposit from three-dimensional renderings of AC, VC, CA1, and mPFC images following combined GENUS versus no stimulation controls (Figure 6D and E, *far right* inset, Supplement Videos 1 and 2, Methods). We observed a significant increase in the number of microglia per plaque in AC (48.88±0.651%), VC (31.56±1.11%), and mPFC (38.64±0.959%) (Figure 6I), and a non-significant increase in CA1 (33.05±2.65%). In contrast, auditory or visual GENUS alone had no significant effect on the number of microglia per plaque versus no stimulation controls in any brain region (Figure S7F and J). Overall, our findings show that combined GENUS elicits a unique microglia response that extends to mPFC, and is not seen with auditory or visual stimulation alone.

We next addressed the frequency-specificity of microglia response in AC, CA1, and mPFC using auditory GENUS, combined GENUS, 80 Hz A+V, or random frequency A+V stimulation. We observed significant increases in microglia number and cell body diameter with decreased average processes length in AC and CA1 following auditory and combined GENUS, but not auditory or A+V stimulation at other frequencies, compared to no stimulation controls. Only combined GENUS elicited a microglia response in mPFC, but not auditory GENUS, nor auditory or A+V stimulation at other frequencies, versus no stimulation controls (Figure S7K–M). We further examined the frequency-specificity of astrocyte reactivity in AC and CA1 using auditory GENUS, combined GENUS, 80 Hz A+V, or random frequency A+V stimulation. Auditory GENUS increased the number of reactive-like astrocytes in both areas, as before (Figure 4H–K). Combined GENUS, but not other frequency A+V groups, elicited a significant increase GFAP-positive astrocytes in AC (63.7 ± 4.3%) and non-significant increase in S100B-positive astrocytes (27.8 ± 2.1%) (Figure S7N, O). We observed non-significant increase in reactive-like astrocytes in CA1 (GFAP: 17.2±2.1%; S100B: 21.6 ± 2.8%) after combined GENUS, but not other frequency A+V groups, versus no stimulation controls (Figure S7O).

Taken together, these results demonstrate that auditory and combined GENUS elicit profound glial responses in primary sensory cortices and HPC, with the latter further impacting mPFC. Moreover, these effects are specific to A+V stimulation at 40 Hz

Concurrent auditory and visual GENUS, but not auditory or visual alone, reduces amyloid load in the mPFC

Our observation of a microglial response in AC, VC, CA1, and mPFC led us to investigate whether combined GENUS could change amyloid levels in those regions. Immunostaining for Aβ (D54D2) revealed reduced plaque area (AC: 56.34±6.3%; VC: 71.50±6.5%; CA1:

69.73±6.4%) and number (AC: 50.02±3.7%; VC: 50.60±10.9%; CA1: 48.80±11.1%) following combined GENUS, versus no stimulation controls. Combined GENUS uniquely reduced plaque area (59.64±8.7%) and number (48.2±0.07%) in mPFC (Figure 7A–D), whereas neither auditory nor visual GENUS alone affected amyloid in mPFC (Figure S7P–U). Multi-comparisons between frequencies and between stimuli modalities in the same data set showed that combined GENUS had significant effects in the mPFC when compared to auditory or visual GENUS alone, and summed auditory and visual stimulations (Supplement Table 1, Figure S7Y and Z). Amyloid reduction in mPFC is frequency-specific, as we observed no significant differences in amyloid plaque area nor number with 80 Hz A+V or random A+V stimulation (Figure 7C and D). We carried out Aβ-ELISA to support our immunostaining results and found that combined GENUS reduced $A\beta_{1-42}$ levels in AC, HPC, as well as mPFC (soluble $A\beta_{1-42}$: 59.58±7.2%; insoluble $A\beta_{1-42}$: 34.17±8.2%) (Figure 7E and F) which was not affected by auditory GENUS alone (Figure S7V and W). Additionally, A+V stimulation at 8 Hz and random frequency did not impact $A\beta_{1-42}$ levels in AC, HPC, and mPFC, compared to no stimulation controls (Figure S7V and W). Immunostaining for $A\beta_{1-42}$ (12F4) showed a unique reduction in amyloid in mPFC after combined GENUS (but not auditory GENUS alone), and no effect of 80 Hz A+V or random frequency A+V stimulation across all three brain regions, compared to their respective no stimulation controls (Figure S7X). In sum, these results demonstrate that combined GENUS uniquely reduces amyloid in mPFC (in contrast to auditory or visual GENUS alone), and that this effect is specific to A+V stimulation at 40 Hz.

To gauge how combined GENUS impacts amyloid plaque abundance on a larger scale, we next performed whole brain SHIELD processing in 6-month-old 5XFAD mice followed by immunostaining for β-amyloid (D54D2) (Methods). Analysis of amyloid plaques in neocortex revealed significant reductions in total plaque volume (37%) and number (34%) after 1 week of combined GENUS versus no stimulation controls (Figure 7G–J, Supplement Videos 3 and 4). These results suggest that combined GENUS may be able to effect widespread reductions of amyloid across broad cortical regions.

Discussion

In this study, we applied the GENUS approach with auditory tones repeating at 25 ms intervals (40 Hz) to effect gamma entrainment and reduce AD pathology in brain regions beyond primary sensory cortex. A key result of auditory GENUS was improved hippocampal-dependent recognition and spatial memory tasks in 5XFAD mice. Alongside significant reductions in amyloid load in AC and HPC, we also observed responses in microglia, astrocytes, and vasculature. Additionally, we show that combined auditory and visual GENUS had unique effects from either sensory modality alone, and reduced amyloid in mPFC and broader cortical regions.

Slow auditory click-train stimuli can elicit a synchronized, phase-locked spiking response from AC neurons although each click becomes more modulatory as the frequency increases (Ma et al., 2013). Consistent with these results, we found that AC neurons entrain to tones repeating at 20 Hz, 40 Hz, and 80 Hz and that for faster frequencies, neurons fire in response to a smaller fraction and at a wider range of phases relative to individual tones. Although

there is extensive evidence that CA1 and mPFC neurons can respond to sensory cues including auditory stimuli (Aronov et al., 2017), (Mears et al., 2006), (Miller and Freedman, 1995), we show for the first time that 40 Hz auditory, or A+V, stimulation elicits small but significant firing rate entrainment at 40 Hz in these brain regions (Figure 1B, H, and N and Figure 6A–C). As in AC, single units in CA1 and mPFC show modulation and fired as a function of stimulus phase although they do not fire in response to every pulse. Weaker spiking modulation may be expected in HPC and mPFC as sensory inputs reach these regions through multiple indirect pathways which likely low-pass filter spiking entrainment.

Studies of rate coding show that neurons can encode click trains using firing rate without synchronizing to the stimulus (Lu et al., 2001) Ma et al., 2013). In each brain region, we found that some neurons fire at a different rate depending on the frequency of the auditory train, although the population as a whole did not fire more or less to the different stimulation frequencies (Figure 1F, L, and R and Figure S6D, K, and R). Therefore, we conclude that our observed changes - in microglia, astrocytes, vasculature, and amyloid levels, as well as behavioral performance - in response to 40 Hz auditory stimulation, but not other frequencies, cannot be explained by overall changes in firing rate.

Microglia display an array of responses, ranging from neurotoxic inflammation to phagocytic to neuroprotective, and their dysfunction is known in AD (Heneka et al., 2014, Wolf et al., 2017). Building on our previous study using visual stimuli (Iaccarino et al., 2016), we show here that auditory GENUS induces a microglia morphological response, indicative of increased Aβ-uptake, in primary sensory cortex as well as HPC (Figure 4A and B). Combining auditory and visual GENUS elicited unique effects of microglia clustering around amyloid plaques, and impacted mPFC in addition to AC and HPC (Figure 6D, E, I). Our results also indicates a range in microglial response that can be elicited by GENUS (Ransohoff and Cardona, 2010), and is supported by accumulating evidence that microglia are heterogeneous and display a spectrum of activated states (Walker and Lue, 2015, Mathys et al., 2017), (Keren-Shaul et al., 2017).

We further investigated effects of GENUS on astrocytes, another primary glial cell type, and found an increase in astrocytes that were positive for markers of reactivity, such as GFAP and S100B (Figure 4H–K, Figure S7N–O). Astrocytes are known to be intermediaries between neuronal activity and regulation of blood flow (Attwell et al., 2010, Filosa and Iddings, 2013). Indeed, we observed an increase in vascular dilation following auditory GENUS (Figure 5A–C). Significantly, mice were sacrificed and analyzed 24 hr post-stimulus, suggesting that vascular changes following GENUS may not be solely due to immediate stimulus response. Vascular clearance, such as through LRP1, may be an additional route for reduced amyloid levels in the brain and, consistent with this hypothesis, we observed increased Aβ-LRP1 co-localization following auditory GENUS (Figure 5D–F).

Our results indicating increased Aβ-uptake by microglia, vascular-dilation response, and potential amyloid transvascular transport all suggest an enhancement in Aβ clearance by auditory GENUS through multiple mechanisms. An intriguing finding is that combined GENUS reduced amyloid load uniquely in mPFC (Figure 7A–F) compared to auditory or visual GENUS alone, and summed auditory and visual stimulations (Figure S7Y and Z,

Supplement Table 1). Whole brain SHIELD revealed a reduction in amyloid load across the whole cortex following combined GENUS versus no stimulation controls (Figure 7G–J), and suggests the potential for combined GENUS to ameliorate AD-like pathology spanning a larger network. However, it remains to be seen if the effects of multi-sensory GENUS on Aβ are synergistic or simply additive through individual sensory modalities.

A major finding from our study is the improvement of hippocampus-dependent cognitive function in spatial and recognition memory tasks in AD model mice following auditory GENUS (Figure 2). Together with our previous study (Iaccarino et al., 2016), our overall findings suggest that GENUS elicits effects across multiple cell types – neurons, microglia, astrocytes, and vasculature - and brain regions to drive the attenuation of AD-related pathology in a circuit-wide manner that is consistent with improved cognitive function. It remains unknown how GENUS relates to endogenous gamma and, for example, whether GENUS affects the capacity for information transmission and sensory processing between neuronal systems (Fries et al., 2001, Fries, 2009, Knoblich et al., 2010). Importantly, because our experiments were performed in AD mouse models, future studies are essential to determine whether the benefits of our non-invasive GENUS approach is translatable to humans.

STAR Methods

Contact for Reagent and Resource Sharing

Further information and requests for resources and reagents should be directed to the Lead Contact, Li-Huei Tsai (lhtsai@mit.edu).

Experimental Model and Subject Details

Animals—All animal work was approved by the Committee for Animal Care of the Division of Comparative Medicine at the Massachusetts Institute of Technology and by the Institutional Animal Care and Use Committee at Georgia Institute of Technology. Mice were housed in groups no larger than five on a standard 12-hour light/12-hour dark cycle; all experiments were performed during the light cycle. Electrophysiology experiments were performed at Georgia Institute of Technology, male (1–3 month-old) WT mice (C57Bl/6) were obtained from the Jackson laboratory. Mice were housed on a reverse 12 h light/12 h dark cycle and all experiments were performed during the dark cycle. Food and water were provided without restriction. For all experiments, mice from the same litter were divided into different conditions, respectfully. If additional groups were added, respective controls were always repeated concurrently.

Method Details

Surgical procedures—Adult (2–3 month-old) mice were anesthetized with isoflurane and fixed in a stereotaxic frame. Ophthalmic ointment (Puralube Vet Ointment, Dechra) was applied to the eyes, and the scalp was shaved and sterilized with povidone-iodine (Dynarex) and 70% ethanol. A custom stainless steel headplate was fixed using dental cement (C&B Metabond, Parkell) and the target craniotomy site for LFP recordings was marked on the skull (in mm, from bregma: −2.0 anterior/ posterior, +/−1.8 medial/lateral for targeting CA1,

−2.0 to −3.0 anterior/ posterior, +/−1.8 medial/lateral for targeting auditory cortex, and +1.3 to +1.4 anterior/posterior, +/− 1.0 medial/lateral for targeting prefrontal cortex). A craniotomy was later performed in 3–8 month-old mice. The day before or day of the first recording session, craniotomies (200–500μm diameter) were made by thinning the skull with a dental drill and then making a hole with a 27-gauge needle. When not recording, the craniotomy was sealed with a sterile silicon elastomer (Kwik-Sil WPI).

Electrophysiology recordings—During recordings, head-fixed animals ran on an air-floating 8-inch spherical treadmill. All animals had previously learned to maneuver on the treadmill until they were comfortable while occasionally receiving sweetened condensed milk (1:2 water dilution). Animals were on the ball for a maximum of 5 hours and had multiple periods of running and rest during this time. Single shank 32-channel probes (NeuroNexus) were advanced to the target location. Recording sites spanned 250 μm. For auditory cortex recordings, the probe was advanced at a 45° angle from vertical parallel to the coronal plane to a depth of 3–4.15mm. A series of 50 ms tones of 5, 10, 15, and 20 kHz were presented to detect auditory response in the mean LFP. For CA1 recordings, the probe was advanced vertically through the craniotomy to a depth of 1.14 – 2.05mm until hippocampal pyramidal layer electrophysiology characteristics were observed (large theta waves and sharp wave ripples, 150+ μV spikes on multiple channels). For prefrontal cortex recordings, the probe was advanced at a 20° angle from vertical, at a 49° angle from the coronal plane to a depth of 1.48–2.15mm. If data were collected at multiple depths during the same recording session; new depths were mapped in order to ensure the location of the recording sites remained in the target location (n = 9 recording depths from 9 sessions in 5 mice for AC and 12 recording depths from 10 sessions in 5 mice for CA1, n = 7 recording depths from 7 sessions in 4 mice for mPFC). Data were acquired with a sampling rate of 20 kHz using an Intan RHD2000 Evaluation System using a ground pellet as reference.

Auditory and visual stimuli for electrophysiology recordings—Animals were presented with 10 s stimulation blocks interleaved with 10 s baseline periods. Stimulation blocks rotated between auditory-only or auditory and visual stimulation at 20 Hz, 40 Hz, 80 Hz, or with random stimulation (pulses were delivered with randomized inter-pulse intervals determined from a uniform distribution with an average interval of 25 ms). Stimuli blocks were interleaved to ensure the results observed were not due to changes over time in the neuronal response. 10 s long stimulus blocks were used to reduce the influence of onset effects, and to examine neural responses to prolonged rhythmic stimulation. All auditory pulses were 1 ms-long 10 kHz tones. All visual pulses were 50% duty cycle of the stimulation frequency (25 ms, 12.5 ms, or 6.25 ms in length). For combined stimulation, auditory and visual pulses were aligned to the onset of each pulse.

Prefrontal cortex histology—During the final mPFC recording in each animal, the probe was coated with DiI and inserted to target depth. Mice were transcardially perfused with 4% paraformaldehyde in phosphate buffered saline (PBS) under anesthesia (isoflurane), and the brains were post-fixed overnight in 4% paraformaldehyde in 1xPBS. Brains were sectioned 100 μm thick with a Leica VT1000S vibratome (Leica). Sections were stained with 0.2% 1mMol DAPI in 1xPBS and mounted onto microscopy slides with Vectashield

mounting medium. Images were acquired on a Zeiss Axio Observer Z1 inverted epifluorescent microscope with the accompanying Zen Blue 2 software.

Spike sorting and single unit stability—Spike detection and sorting was carried out using MountainSort automated spike sorting followed by manual curation based on visual inspection of waveforms and cross-correlograms (Chung et al., 2017). Prior to manual curation, quality thresholds were applied to only include units with peak SNR greater than or equal to 1, less than 10% overlap with noise, and greater than 95% isolation against other units which resulted in well-isolated single units. To account for periods of instability in the recordings during which single units were lost, stability criteria were applied such that only stable periods (no sudden loss of a single unit's firing rate) would be considered in analysis. Firing rate (FR) for each unit was computed over the course of the recording session. Firing rate was clustered into two distributions, low FR and high FR, using k-means clustering. For units with FR that dropped below 10% of the high FR mean, further analyses identified a stable recording period defined as the longest length of time that the FR was 2 standard deviations above the low FR mean.

LFP—LFP was obtained by downsampling raw traces to 2kHz and bandpass filtering between 1–300Hz.

Power spectrum—Power spectral density analysis was performed using multitaper methods from the Chronux toolbox (time-bandwidth product = 3, number of tapers = 5). LFP traces were divided into 10s trials of each stimulation condition. The average power spectral density was computed for each animal (within the same recording day and recording depth) over these trials, referencing to a ground pellet in saline above the skull. Power spectral density analysis was initially computed for all recording sites in AC, CA1, and mPFC. From each recording depth, the traces with the largest 40 Hz peak in response to 40 Hz flicker stimuli were included in the analysis. The per-depth traces displayed in the presented data had the largest 40 Hz peak in response to auditory flicker stimuli.

Firing during flicker stimulation—The single unit peri-stimulus time histograms (PSTH) for each stimulus frequency encompassed two stimulus cycles (where one cycle = $\frac{1}{stimulus\ frequency}$sec), with 10 bins per cycle, to show spiking across trains of stimuli. Displaying spiking modulation over multiple cycles is typical for displaying modulation by oscillations (Csicsvari et al., 1999). PSTHs were computed for all single units by binning spikes for 1 stimulus cycles before and after the start of each light-on or audio-on pulse. No stimulation (baseline) histograms were calculated using randomly distributed pulse times, as in the random stimulation condition. Firing rate was computed in each bin by dividing the number of spikes per bin by the total time in that bin (the total number of pulses times the bin size). To quantify firing rate periodicity in relation to the stimulus frequency, the time interval between firing rate peaks was calculated for all single unit histograms. The peaks of each PSTH was the maximum firing rate within one stimulus interval. To quantify firing rate modulation by the stimulus and compute circular statistics, peri-stimulus spike times were converted into radians: $(peri - stimulus\ spike\ tine) * 2\pi * (stimulus\ frequency)$ and vector strengths and Rayleigh statistics were computed. Vector strength was computed

using methods from the CircStat toolbox; the Rayleigh statistic was computed using the equation RS = $2nVS^2$, where n is total spike count, and VS is vector strength (Berens, 2009), Ma et al. 2013). Differences in vector strength and Rayleigh statistic values were computed by taking the differences in these values between stimulus conditions for each unit. Heat maps showing the firing rate response to flicker for all recorded single units were computed over four consecutive stimulus cycles. In order to show the response of all neurons, we show four consecutive stimulus cycles of each stimulation period. To do this, we aligned the 10s presentation periods of each stimulus condition, and then excluded the first 100ms of each presentation period to prevent onset effects from obscuring entrainment. Then, we averaged spiking response over the next four stimulus cycles (200 ms for 20 Hz, 100 ms for 40 Hz, and 50 ms for 80 Hz) to obtain the firing rate response to flicker. Firing rate for each single unit was computed in 1ms bins, smoothed with a gaussian windows proportional to each stimulus frequency ($N = \frac{1}{Stimulus\ frequency}$sec, $\alpha = 3$), and z-scored. Neurons were aligned by their average stimulus phase preference in the analyzed four cycles.

Mean Firing Rate—Mean firing rate was computed for each single unit for each stimulus condition. Only stable periods for each unit contributed to the mean FR calculation (see Spike sorting and single unit stability, above). Difference in mean firing rate between stimulus conditions was computed within each unit by taking the difference in mean FR in each condition for that unit.

40 Hz visual flicker stimulation protocol—For biochemical and Immunohistochemical analysis, 5XFAD mice were placed in a dark chamber illuminated by a light-emitting diode (LED) bulb and were exposed to one of four stimulation conditions: dark, 8 Hz, 40 Hz (12.5 ms light on, 12.5 ms light off, 60 W), or random (light pulses were delivered with a random interval determined by a uniform distribution with a mean of 25 ms) stimulation for 1-hour for seven days.

40 Hz auditory tone train stimulation protocol—For biochemical, Immunohistochemical, or behavioral analysis, 5XFAD, APP/PS1, or P301S mice were placed in a dimly lit chamber in a quiet room insulated with sound-proof foam (McMaster-Carr, 5692T49). Speakers (AYL, AC-48073) were placed out-of-reach from the mouse above the chambers. Mice were exposed to one of five stimulation conditions: no tones, tones at 8 Hz, tones at 40 Hz, tones at 80 Hz, or tone delivered at random (auditory tones were delivered with a random interval determined by a uniform distribution with a mean of 25ms) stimulation. Tones for the stimulation conditions consisted of a 10 kHz tone that was 1 ms in duration and delivered at 60 dB. For electrophysiology recordings, after probe placement, the lights in the room were turned off and the animals were presented with alternating 10 s periods of audio-only and visual-audio stimulation interleaved with 10 s periods of no light or tones. For audio-only stimulation, a 10 kHz tone was played at 40 Hz with a 4% duty cycle. For visual-audio stimulation, the audio stimulation was accompanied with surrounding light flickered at 40 Hz for 10 s periods with a 50% duty cycle. Stimuli were presented in this manner for 20 min sessions, with 1–10 min pauses in between sessions to check on the animals' behavior.

Concurrent 40 Hz auditory and visual stimulation protocol—For biochemical, Immunohistochemical, or behavioral analysis, 5XFAD mice were placed in a dark chamber illuminated by an LED bulb and exposed to an auditory tone train, simultaneously. Mice were exposed to one of four stimulations: dark/quiet, 40 Hz light flicker, 40 Hz auditory tone train, concurrent 40 Hz light flicker and auditory tone, or random light flicker/tone stimulations.

Immunohistochemistry—Mice were transcardially perfused with 4% paraformaldehyde in phosphate buffered saline (PBS) under anesthesia (2:1 of ketamine/xylazine), and the brains were post-fixed overnight in 4% paraformaldehyde in PBS. Brains were sectioned 40 μm thick with a Leica VT1000S vibratome (Leica). Sections were permeabilized and blocked in PBS with 0.3% Triton X-100 and 10% donkey serum at room temperature for 2-hours. Sections were incubated overnight at 4°C in primary antibody containing PBS with 0.3% Triton X-100 and 10% donkey serum. Primary antibodies were: anti-β -amyloid (Cell Signaling Technology; D54D2), anti-Iba1 (Wako Chemicals; 019–19741), anti-glial fibrillary acidic protein (GFAP)(Abcam; ab4674), anti-S100B (Abcam; ab868), anti-LRP1 (Abcam; 28320), DyLight 488 labeled Lycopersicon Esculentum (tomato) lectin (Vector laboratories; DL-1174), anti-amyloid oligomer (Millipore Sigma; AB9234), anti-phospho-tau (Ser396) (Cell Signaling Technology; 9632), anti-phosphotau (Thr181) (Cell Signaling Technology, 12885), Hoechst 33342 (Thermo Fisher Scientific; H3570). The anti-Aβ antibody 12F4 was used because it does not react with APP, allowing us to determine whether our labelling was specific to Aβ, as well as allowing for co-labelling with Iba1. Anti-amyloid oligomer antibody AB9234 was used for co-labelling with LRP1. The following day, brain sections were incubated with fluorescently conjugated secondary antibodies (Jackson ImmunoResearch) for 2 hours at room temperature, and nuclei were stained with Hoechst 33342 (Invitrogen). Images were acquired using a confocal microscope (LSM 710; Zeiss) with a 40× objective at identical settings for all conditions. Images were quantified using ImageJ 1.42q by an experimenter blind to treatment groups. For each experimental condition, two coronal sections from each animal were used for quantification. Scale bars are 50 μm unless otherwise noted in figure legends. ImageJ was used to measure the diameter of Iba1+ cell bodies and to trace the processes for length measurement. In addition, the Coloc2 plugin was used to measure co-localization of Iba1 and Aβ. Microglia processes arborization was quantified using Imarisx64 8.1.2 (Bitplane, Zurich, Switzerland). The ‘analyze particles’ function in ImageJ was used for counting plaque number and area, deposits of at least 10 μm were included and a set threshold was used for both control and experimental groups.

Vasculature- Aβ colocalization analysis—ImarisColoc module was used to quantify colocalzation of signal between two separate source channels (i.e. Lectin and AB, Lectin and LRP1) in 3D. These source channels were thresholded to mask any intensity coming from noise or background signal. ImarisColoc then generates a new channel containing only voxels that colocalize within the thresholds set for the source channels, and presents the associated statistical analyses.

Microglia-Aβ clustering analysis—IMARIS was used to analyze the microglial clustering pattern around amyloid plaques in 40uM slices. The surfaces module was utilized to detect and 3D render plaques (red) based on 12F4 signal. Iba1-positive microglia were then counted using the spots module, placing a sphere at the soma of each cell (green). Finally, the Spots Close To Surface XTension was run to find the subset of spots that are closer to the surface objects than the defined 25uM threshold, and exclusion of spots that fall outside this range. The algorithm measures the distance from the center of the spot to the nearest point of the surface object in 3D space, allowing for the quantification of microglial aggregation near plaques.

CLARITY immunostaining in brain slices—Mice were perfused with ice-cold PBS (1X) followed by ice-cold 4% PFA, 1% glutaraldehyde in 1xPBS. Brains were dissected out and post-fixed in 4% PFA/1% glutaraldehyde solution for 72 hours at 4°C. Fixation was terminated by incubating brains in inactivation solution (4% acrylamide, 1 M glycine, 0.1% triton-X100 in 1X PBS) for 48 hours at RT. After washing in 1xPBS, brains were sliced into 100uM coronal sections on a vibratome (Leica VT100S) in 1xPBS. Sections containing regions of interest (i.e. auditory cortex and hippocampus) were selected, with reference to the Allen Mouse Brain Atlas, and incubated in clearing buffer (pH 8.5–9.0, 200mM sodium dodecylsulfate, 20mM lithium hydroxide monohydrate, 4mM boric acid in ddH2O) for 2–4 hours, shaking at 55°C. Cleared sections were washed 3 ×15mins in 1xPBST (0.1% Triton-X100/1XPBS) and put into blocking solution (2% bovine serum albumin/1xPBST) overnight at RT. Subsequently, three 1hour washes in 1x PBST were performed, shaking at RT. Sections were incubated in weak binding buffer (pH 8.5–9.0, 37.75 mM Na2HPO4, 3.53 mM KH2PO4, 0.02% sodium azide in PBST) for 1 hour at RT, then transferred to primary antibody, diluted to 1:100 in 1x weak binding buffer for 12 hours at 37°C. Reversal buffer (pH 7.4, 37.75 mM Na2HPO4, 3.53 mM KH2PO4 in 0.02% sodium azide in PBST) is then added in even hourly aliquots over 6 hours, to equal the volume of primary antibody solution plus the volume of the tissue. Another set of 3×1 hour washes in 1xPBST was conducted before sections were incubated for 12 hours at RT, in a mixture of Hoechst 33258 (1:250) (Sigma-Aldrich, 94403) and secondary antibody (1:100) in 1xPBS. Sections were then washed overnight in 1xPBS and incubated in RIMS (Refractive Index Matching Solution: 75g Histodenz, 20mL 0.1M phosphate buffer, 60mL ddH2O) for 1 hour at RT prior to mounting. Brain sections were mounted onto microscopy slides with coverslips (VWR VistaVision, VWR International, LLC, Radnor, PA) in RIMS. Images were acquired on a Zeiss LSM 880 microscope with the accompanying Zen Black 2.1 software (Carl Zeiss Microscopy, Jena, Germany). Z-stack images were taken with a step size of 0.4–0.5 μm, pixel dwell 4.1 ms, averaging of 2, resolution 1024×1024 suitable for 3D reconstruction. Imarisx64 8.3.1 (Bitplane, Zurich, Switzerland) was used for 3-D rendering and analysis.

Whole mouse brain processing and clearing—5XFAD mouse brains were processed according to the SHIELD protocol (Park et al., 2018). Briefly, 5XFAD mice were transcardially perfused with ice-cold PBS followed by 20 mLs of SHIELD-OFF solution containing 4% PFA. Brains were dissected and post-fixed in the same solution for 24 hours at 4°C. Brains were then incubated overnight in SHIELD-OFF solution without PFA at 4°C. Brains were then incubated in the SHIELD-ON solution for 24 hours at 37°C. Following

fixation, brains were incubated in an aqueous clearing solution containing 200mM sodium doedecyl sulfate (SDS), 20mM lithium hydroxide monohydrate, 40mM boric acid, pH 8.5–9.0. Brains were then cleared using SmartClear Pro (LifeCanvas Technologies, Cambridge, MA) based on stochastic electrotransport (Kim et al., 2015) for several days, until transparent.

Immunostaining of cleared whole hemispheres—Cleared hemispheres were stained with 15ul of beta-amyloid antibody conjugated with Alexa Fluor-488 (CST, #51374) over 2 days, using a eTANGO, a modified stochastic electrotransport method (Kim et al., PNAS, 2015).

Light-sheet microscopy—Immunostained samples were incubated with hProtos (3g diatrizoic acid, 5g N-methyl-d-gludamine, 125g iohexol in 105ml DI-water) for optical clearing and then mounted to acrylic holder using 2% low-temperature melting agarose in hProtos. Custom-made light-sheet microscope equipped with 10× CLARITY-optimized objective was used to image whole hemispheres using the 488 channel for beta-amyloid visualization and the 647 channel for autofluorescence.

Cleared whole brain image processing, plaque detection, and atlas alignment —Acquired image data were illumination corrected using CIDRE, an open-source software package implemented in Matlab, and the resulting processed images were stitched together using Terastitcher. Imaris (Bitplane, http://www.bitplane.com/imaris/imaris) was used for 3D visualizations, and ImageJ (NIH, http://imagej.nih.gov/ij/) was used to create representative slice-by-slice 2D visualizations. Automated plaque detection was performed using a combination of the open-source ClearMap software, a custom cell classification neural network model, and Elastix. Candidate plaques were located as “spots” with ClearMap’s spot detection module. First, background subtraction was done slice-by-slice by using a grey-scale morphological top-hat transformation with a disk structure element with major and minor diameter pixel sizes of (21,21). Next, local maxima of the data are detected by applying a 3D maxima filter with disk structure element of size (7,7,4), and these local maxima are filtered with an intensity threshold of 100. The pixel volumes corresponding to each spot center location are also computed using a 3D watershed transform with spot centers as seed points. All candidate plaques with volume less than a sphere with 10-micron diameter were then filtered out. True plaques were identified from the candidate plaques using a convolutional neural network (CNN) model as a categorical plaque / non-plaque classifier implemented in Keras (https://keras.io/) with a Theano backend (https://github.com/Theano/Theano). The CNN input is a 32-by-32 pixel bounding box centered at a candidate plaque center, and the output is a two element one-hot vector representing the plaque and non-plaque categories. The architecture consists of 12 total convolutional layers, each with a rectified linear unit (ReLU) activation and followed by batch normalization: 3 with 64 2×2 kernels, 3 with 128 2×2 kernels, followed by 3 with 192 2×2 kernels, 1 with 256 2×2 kernels, 1 with 256 1×1 kernels, and 1 with 2 1×1 kernels. 2×2 subsampling is done after the third, sixth, and ninth convolutional layer, and Dropout with a rate of 0.5 is applied after the last nine convolutional/batch normalization layers for regularization. After the final convolutional layer, global average pooling followed by softmax activation is applied to

generate the final categorical vector. During training, a categorical cross entropy loss was used with the Adam optimizer with default parameters. The CNN was trained for 400 epochs with batch size of 64 on ~10,000 manual plaque annotations augmented with random rotations, shears, and reflections using the Keras Image Data Generator. The resulting model was then used to classify plaques from detected spots for all samples. To perform atlas alignment, autofluorescence channel images were first downsampled to the atlas resolution, and then Elastix was used to calculate affine and B-spline transformation parameters to do 3D image registration, with the resampled autofluorescence image as the fixed image and the atlas as moving image. The resulting alignment parameters were applied on the plaque locations (output from the CNN model) to transform the plaques into the atlas space, after which a CSV file with plaque count and volume information for each brain region (segmentation according to the Allen Brain Atlas) is generated.

Western blot—Hippocampus and auditory cortex from 6-month-old tau P301S mice were dissected and homogenized in RIPA buffer (50 mM Tris, pH 8.0, 150 mM NaCl, 1% NP-40, 0.5% sodium deoxycholate, 0.1% SDS) containing protease and phosphatase inhibitors. Lysates were incubated on ice for 15 min and spun at 12,000 RPM for 15 minutes. Then, supernatants were transferred to fresh tubes and analyzed for protein concentration (Bio-Rad Protein Assay). Equal amounts of protein (20 ug/lane) was resolved on a SDS-polyacrylamide gel and blotted onto a PVDF membrane. This membrane was incubated in blocking buffer containting 20 mM Tris-HCl (pH 7.4), 150 mM NaCl, and 0.1% (v/v) Tween 20 (TBS-T) plus 5% dry milk (m/v) for 1 h at room temperature followed by incubation overnight at 4 °C in primary antibodies and then secondary antibodies at room temperature for 1 hour. Primary antibodies were anti-phospho-tau (Ser396) and anti-phospho-tau (Thr181). Secondary antibodies were LI-COR IRDye secondary antibodies. Signal intensities were quantified using ImageJ 1.46a and normalized to values of total tau Tau5 (Thermo Fisher Scientific; AHB0042).

Tau seeding activity assay—2-month old tau P301S brain sections were homogenized in 1× TBS supplemented with protease inhibitors (Roche complete mini tablets) using a probe sonicator (30% power; 15 pulses). After sonication, the lysates were centrifuged at 14,000 × g for 15 min to eliminate large, insoluble material. The supernatant was stored at −80°C and used for all future experiments. Protein concentration was determined using a Bio-Rad Protein Assay Dye. Fluorescence resonance energy transfer (FRET) biosensor cell lines described previously (Holmes et al., 2014) were provided by Marc I. Diamond. Cells were grown in DMEM (Invitrogen) augmented with 10% FBS and 1× penicillin/streptomycin and maintained at 37°C and 5% CO2 in a humidified incubator. For the assay, cells were plated in a 96-well plate at a density of 40,000 cells/well. Sixteen hours later, at 50% confluence, brain homogenate samples were transduced into cells using 1.2 μl Lipofectamine/well. After a 24 h incubation at 37°C, cells were harvested with 0.25% trypsin, fixed in 2% PFA (Electron Microscopy Services) for 15 min, and then resuspended in PBS. An LSR II HST-2 flow cytometer was used to measure the FRET signal within each cell. FRET quantification was accomplished using FlowJo version 10 software (TreeStar). Integrated FRET density was derived by multiplying the percentage of FRET-positive cells in each sample by the median FRET intensity of those cells.

ELISA—Primary auditory cortices, medial prefrontal cortices, and hippocampi were isolated from 6-month-old 5XFAD males and subjected to Aβ measurement using $A\beta_{42}$ or $A\beta_{40}$ ELISA kits (Invitrogen) according to the manufacturer's instructions. Insoluble Aβ was treated with 5M guanidine/50 mM Tris HCL (pH 8.0) buffer before ELISA measurement.

Behavioral Experiments

Novel Object Recognition—The novel object recognition (NOR) task consisted of a habituation phase followed by training and testing performed the following day, as previously described (Leger et al., 2013). 24 hours before training, mice were habituated to an open testing arena (40 cm L x 40 cm W x 35 cm H) for 5 min, during which total distance (cm), time in the center (s), and velocity (cm/s) were calculated (TSE Systems). During training, mice were placed into the same box with two identical objects placed in opposite corners. Mice were allowed a total of 20 seconds of object interaction time (within a maximum time frame of 10 minutes), and then immediately removed from the arena. Object memory was tested 1 hr later using the same procedure during training, except one object was replaced with a novel one in its place. Object exploration was recorded when the snout contacted either object and was calculated by a recognition index, $RI=T_{novel}/(T_{novel}+T_{familiar})$, where T_{novel} and $T_{familiar}$ indicate the time spent with the novel and familiar object, respectively.

Novel Object Location—The novel location recognition (NOL) task was performed using the same procedure as the object recognition task, except two identical objects were used for both training and testing, and one object was displaced to a novel location during testing.

Morris Water Maze Test—Spatial reference memory testing was performed in a circular tank (diameter, 1.2m) filled with white opaque water at approximately 22°C. Reference cues consisting of different colors and shapes were placed along the walls surrounding the tank. Within the tank was a fixed platform (diameter, 10cm) located in a target quadrant. During testing, the platform was submerged and the mice were placed into the tank at one of seven points randomly facing the wall of the tank. Mice were provided 60 s to search for the platform, which if not found, were gently guided to it. Animals were kept on the platform for 15 s. Two trials a day were conducted with a 1 hour intertrial interval. Between the trails, mice were gently padded dry and warmed on a heating pad. Mouse behavior was video-recorded using TSE Systems. The escape latency, or the time it took for the mouse to reach the platform, was scored for each trial and averaged per testing day. On day 6, the platform was removed and a memory test (probe test) was performed. The time spent in each of the 4 quadrants and the number of crossing of the area where the platform used to be was recorded. Swimming velocity was recorded automatically.

Quantification and Statistical Analysis

Statistical analysis—Statistical significance between two groups for non-electrophysiology experiments was calculated by two-tailed unpaired Mann-Whitney test. Significance between three groups or more was calculated by Kruskal-Wallis test with

Dunn's multiple comparisons test. Prism 7 software was used to calculate the values. For electrophysiology data, differences between two stimulus conditions were assessed using non-parametric, two-sample Kolmogorov-Smirnov goodness of fit tests to compare circular statistic value distributions or using z-Test for two proportions to compare proportions. The significance of difference distributions was assessed using two-sided Wilcoxon signed rank test for zero median (e.g. differences in firing rates between stimulus conditions). Multiple comparisons were controlled for using the Bonferroni correction. Significance values are $p < 0.05$ (∗), $p < 0.01$ (∗∗), and $p < 0.001$ (∗∗∗) unless otherwise specified. Specific statistical parameters are detailed in the figure legends.

Supplementary Material

Refer to Web version on PubMed Central for supplementary material.

Acknowledgements

We are grateful to members of the Tsai, Singer, and Boyden laboratories for technical assistance, and comments on the paper. This work was supported by A.C.S.: Packard award in Science and Engineering, NIH R01-NS109226, Friends and Alumni of Georgia Tech, Lane Family; A.L.P.: T32 NS007480–18, Fulton County Elder Health Science Fellowship, Wright Family; L.H.T.: Robert and Renee Belfer Family Foundation, Halis Family Foundation, JPB Foundation, NIH RF1-AG047661; K.C.: Burroughs Wellcome Fund Career Awards at the Scientific Interface, Searle Scholars Program, Packard award in Science and Engineering, NARSAD Young Investigator Award, JPB Foundation (PIIF and PNDRF), NCSOFT Cultural Foundation, NIH U01-NS090473; A.J.M.: T32 GM007484 Integrative Neuronal Systems, MIT Champions of the Brain Fellowship, Henry E. Singleton Fellowship; W.G.: William C. and Margaret H. Rousseau Fellowship; V.M.: SITA Foundation Fellowship; H-J.S.: Samsung Fellowship; E.S.B.: MIT Aging Brain Initiative, John Doerr, Edward and Kay Poitras, HHMI-Simons Fellowship, Open Philanthropy, Charles Hieken, NIH R01-EY023173; E.N.B.: NIH R01-GM104948, DP1-OD003646, Department of Anesthesia, Critical Care and Pain Medicine, Massachusetts General Hospital, Boston, Massachusetts.

References

Allen NJ, and Barres BA (2005). Signaling between glia and neurons: focus on synaptic plasticity. Curr Opin Neurobiol 15, 542–548. [PubMed: 16144764]

Aronov D, Nevers R, and Tank DW (2017). Mapping of a non-spatial dimension by the hippocampal-entorhinal circuit. Nature 543, 719–722. [PubMed: 28358077]

Attwell D, Buchan AM, Charpak S, Lauritzen M, Macvicar BA, and Newman EA (2010). Glial and neuronal control of brain blood flow. Nature 468, 232–243. [PubMed: 21068832]

Berens P (2009). CircStat: A MATLAB Toolbox for Circular Statistics. Journal of Statistical Software Vol 31, 1–21.

Bero AW, Yan P, Roh JH, Cirrito JR, Stewart FR, Raichle ME, Lee JM, and Holtzman DM (2011). Neuronal activity regulates the regional vulnerability to amyloid-β deposition. Nat Neurosci 14, 750–756. [PubMed: 21532579]

Canter RG, Penney J, and Tsai LH (2016). The road to restoring neural circuits for the treatment of Alzheimer's disease. Nature 539, 187–196. [PubMed: 27830780]

Cardin JA, Carlén M, Meletis K, Knoblich U, Zhang F, Deisseroth K, Tsai LH, and Moore CI (2009). Driving fast-spiking cells induces gamma rhythm and controls sensory responses. Nature 459, 663–667. [PubMed: 19396156]

Chung JE, Magland JF, Barnett AH, Tolosa VM, Tooker AC, Lee KY, Shah KG, Felix SH, Frank LM, and Greengard LF (2017). A Fully Automated Approach to Spike Sorting. Neuron 95, 1381–1394.e1386. [PubMed: 28910621]

Chung WS, Allen NJ, and Eroglu C (2015). Astrocytes Control Synapse Formation, Function, and Elimination. Cold Spring Harb Perspect Biol 7, a020370. [PubMed: 25663667]

Cirrito JR, Yamada KA, Finn MB, Sloviter RS, Bales KR, May PC, Schoepp DD, Paul SM, Mennerick S, and Holtzman DM (2005). Synaptic activity regulates interstitial fluid amyloid-beta levels in vivo. Neuron 48, 913–922. [PubMed: 16364896]

Csicsvari J, Hirase H, Czurkó A, Mamiya A, and Buzsáki G (1999). Oscillatory coupling of hippocampal pyramidal cells and interneurons in the behaving Rat. J Neurosci 19, 274–287. [PubMed: 9870957]

Filosa JA, and Iddings JA (2013). Astrocyte regulation of cerebral vascular tone. Am J Physiol Heart Circ Physiol 305, H609–619. [PubMed: 23792684]

Fries P (2009). Neuronal gamma-band synchronization as a fundamental process in cortical computation. Annu Rev Neurosci 32, 209–224. [PubMed: 19400723]

Gillespie AK, Jones EA, Lin YH, Karlsson MP, Kay K, Yoon SY, Tong LM, Nova P, Carr JS, Frank LM, et al. (2016). Apolipoprotein E4 Causes Age-Dependent Disruption of Slow Gamma Oscillations during Hippocampal Sharp-Wave Ripples. Neuron 90, 740–751. [PubMed: 27161522]

Hardy JA, and Higgins GA (1992). Alzheimer's disease: the amyloid cascade hypothesis. Science 256, 184–185. [PubMed: 1566067]

Heneka MT, Kummer MP, and Latz E (2014). Innate immune activation in neurodegenerative disease. Nat Rev Immunol 14, 463–477. [PubMed: 24962261]

Holmes BB, Furman JL, Mahan TE, Yamasaki TR, Mirbaha H, Eades WC, Belaygorod L, Cairns NJ, Holtzman DM, and Diamond MI (2014). Proteopathic tau seeding predicts tauopathy in vivo. Proc Natl Acad Sci U S A 111, E4376–4385. [PubMed: 25261551]

Iaccarino HF, Singer AC, Martorell AJ, Rudenko A, Gao F, Gillingham TZ, Mathys H, Seo J, Kritskiy O, Abdurrob F, et al. (2016). Gamma frequency entrainment attenuates amyloid load and modifies microglia. Nature 540, 230–235. [PubMed: 27929004]

Iliff JJ, Wang M, Liao Y, Plogg BA, Peng W, Gundersen GA, Benveniste H, Vates GE, Deane R, Goldman SA, et al. (2012). A paravascular pathway facilitates CSF flow through the brain parenchyma and the clearance of interstitial solutes, including amyloid β. Sci Transl Med 4, 147ra111.

Kanekiyo T, Cirrito JR, Liu CC, Shinohara M, Li J, Schuler DR, Holtzman DM, and Bu G (2013). Neuronal clearance of amyloid-β by endocytic receptor LRP1. J Neurosci 33, 19276–19283. [PubMed: 24305823]

Keren-Shaul H, Spinrad A, Weiner A, Matcovitch-Natan O, Dvir-Szternfeld R, Ulland TK, David E, Baruch K, Lara-Astaiso D, Toth B, et al. (2017). A Unique Microglia Type Associated with Restricting Development of Alzheimer's Disease. Cell 169, 1276–1290.e1217. [PubMed: 28602351]

Kim H, Ährlund-Richter S, Wang X, Deisseroth K, and Carlén M (2016). Prefrontal Parvalbumin Neurons in Control of Attention. Cell 164, 208–218. [PubMed: 26771492]

Kim SY, Cho JH, Murray E, Bakh N, Choi H, Ohn K, Ruelas L, Hubbert A, McCue M, Vassallo SL, et al. (2015). Stochastic electrotransport selectively enhances the transport of highly electromobile molecules. Proc Natl Acad Sci U S A 112, E6274–6283. [PubMed: 26578787]

Kisler K, Nelson AR, Montagne A, and Zlokovic BV (2017). Cerebral blood flow regulation and neurovascular dysfunction in Alzheimer disease. Nat Rev Neurosci 18, 419–434. [PubMed: 28515434]

Leger M, Quiedeville A, Bouet V, Haelewyn B, Boulouard M, Schumann-Bard P, and Freret T (2013). Object recognition test in mice. Nat Protoc 8, 2531–2537. [PubMed: 24263092]

Lu T, Liang L, and Wang X (2001). Neural representations of temporally asymmetric stimuli in the auditory cortex of awake primates. J Neurophysiol 85, 2364–2380. [PubMed: 11387383]

Ma L, Tai X, Su L, Shi L, Wang E, and Qin L (2013). The neuronal responses to repetitive acoustic pulses in different fields of the auditory cortex of awake rats. PLoS One 8, e64288. [PubMed: 23696877]

Mathys H, Adaikkan C, Gao F, Young JZ, Manet E, Hemberg M, De Jager PL, Ransohoff RM, Regev A, and Tsai LH (2017). Temporal Tracking of Microglia Activation in Neurodegeneration at Single-Cell Resolution. Cell Rep 21, 366–380. [PubMed: 29020624]

Mears RP, Klein AC, and Cromwell HC (2006). Auditory inhibitory gating in medial prefrontal cortex: Single unit and local field potential analysis. Neuroscience 141, 47–65. [PubMed: 16675142]

Miller CL, and Freedman R (1995). The activity of hippocampal interneurons and pyramidal cells during the response of the hippocampus to repeated auditory stimuli. Neuroscience 69, 371–381. [PubMed: 8552235]

Morris R (1984). Developments of a water-maze procedure for studying spatial learning in the rat. J Neurosci Methods 11, 47–60. [PubMed: 6471907]

Mosher KI, and Wyss-Coray T (2014). Microglial dysfunction in brain aging and Alzheimer's disease. Biochem Pharmacol 88, 594–604. [PubMed: 24445162]

Oakley H, Cole SL, Logan S, Maus E, Shao P, Craft J, Guillozet-Bongaarts A, Ohno M, Disterhoft J, Van Eldik L, et al.(2006). Intraneuronal beta-amyloid aggregates, neurodegeneration, and neuron loss in transgenic mice with five familial Alzheimer's disease mutations: potential factors in amyloid plaque formation. J Neurosci 26, 10129–10140. [PubMed: 17021169]

Palop JJ, Chin J, Roberson ED, Wang J, Thwin MT, Bien-Ly N, Yoo J, Ho KO, Yu GQ, Kreitzer A, et al. (2007). Aberrant excitatory neuronal activity and compensatory remodeling of inhibitory hippocampal circuits in mouse models of Alzheimer's disease. Neuron 55, 697–711. [PubMed: 17785178]

Park YG, Sohn CH, Chen R, McCue M, Yun DH, Drummond GT, Ku T, Evans NB, Oak HC, Trieu W, et al. (2018). Protection of tissue physicochemical properties using polyfunctional crosslinkers. Nat Biotechnol

Rager G, and Singer W (1998). The response of cat visual cortex to flicker stimuli of variable frequency. Eur J Neurosci 10, 1856–1877. [PubMed: 9751156]

Ransohoff RM, and Cardona AE (2010). The myeloid cells of the central nervous system parenchyma. Nature 468, 253–262. [PubMed: 21068834]

Rodríguez JJ, Olabarria M, Chvatal A, and Verkhratsky A (2009). Astroglia in dementia and Alzheimer's disease. Cell Death Differ 16, 378–385. [PubMed: 19057621]

Saijo K, and Glass CK (2011). Microglial cell origin and phenotypes in health and disease. Nat Rev Immunol 11, 775–787. [PubMed: 22025055]

Seeley WW, Crawford RK, Zhou J, Miller BL, and Greicius MD (2009). Neurodegenerative diseases target large-scale human brain networks. Neuron 62, 42–52. [PubMed: 19376066]

Selkoe DJ, Yamazaki T, Citron M, Podlisny MB, Koo EH, Teplow DB, and Haass C (1996). The role of APP processing and trafficking pathways in the formation of amyloid beta-protein. Ann N Y Acad Sci 777, 57–64. [PubMed: 8624127]

Sohal VS, Zhang F, Yizhar O, and Deisseroth K (2009). Parvalbumin neurons and gamma rhythms enhance cortical circuit performance. Nature 459, 698–702. [PubMed: 19396159]

Spellman T, Rigotti M, Ahmari SE, Fusi S, Gogos JA, and Gordon JA (2015). Hippocampal-prefrontal input supports spatial encoding in working memory. Nature 522, 309–314. [PubMed: 26053122]

Sperling RA, Dickerson BC, Pihlajamaki M, Vannini P, LaViolette PS, Vitolo OV, Hedden T, Becker JA, Rentz DM, Selkoe DJ, et al. (2010). Functional alterations in memory networks in early Alzheimer's disease. Neuromolecular Med 12, 27–43. [PubMed: 20069392]

Storck SE, Meister S, Nahrath J, Meißner JN, Schubert N, Di Spiezio A, Baches S, Vandenbroucke RE, Bouter Y, Prikulis I, et al. (2016). Endothelial LRP1 transports amyloid-β(1–42) across the blood-brain barrier. J Clin Invest 126, 123–136. [PubMed: 26619118]

Verret L, Mann EO, Hang GB, Barth AM, Cobos I, Ho K, Devidze N, Masliah E, Kreitzer AC, Mody I, et al. (2012). Inhibitory interneuron deficit links altered network activity and cognitive dysfunction in Alzheimer model. Cell 149, 708–721. [PubMed: 22541439]

Vorhees CV, and Williams MT (2006). Morris water maze: procedures for assessing spatial and related forms of learning and memory. Nat Protoc 1, 848–858. [PubMed: 17406317]

Walker DG, and Lue LF (2015). Immune phenotypes of microglia in human neurodegenerative disease: challenges to detecting microglial polarization in human brains. Alzheimers Res Ther 7, 56. [PubMed: 26286145]

Wolf SA, Boddeke HW, and Kettenmann H (2017). Microglia in Physiology and Disease. Annu Rev Physiol 79, 619–643. [PubMed: 27959620]

Yamamoto J, Suh J, Takeuchi D, and Tonegawa S (2014). Successful execution of working memory linked to synchronized high-frequency gamma oscillations. Cell 157, 845–857. [PubMed: 24768692]

Yankner BA, and Lu T (2009). Amyloid beta-protein toxicity and the pathogenesis of Alzheimer disease. J Biol Chem 284, 4755–4759. [PubMed: 18957434]

Yoshiyama Y, Higuchi M, Zhang B, Huang SM, Iwata N, Saido TC, Maeda J, Suhara T, Trojanowski JQ, and Lee VM (2007). Synapse loss and microglial activation precede tangles in a P301S tauopathy mouse model. Neuron 53, 337–351. [PubMed: 17270732]

Highlights

- Auditory Gamma ENtrainment Using Sensory stimuli (GENUS) boosts hippocampal function
- GENUS affects microglia, astrocytes, and vasculature in auditory cortex and hippocampus
- Auditory plus visual GENUS induces microglia clustering around plaques
- Auditory plus visual GENUS reduces amyloid pathology throughout neocortex

Auditory stimulation combined with light-induced gamma oscillations in the hippocampus CA1 and auditory cortex regions of the brain reduces amyloid levels and improves memory in animal models of Alzheimer's disease.

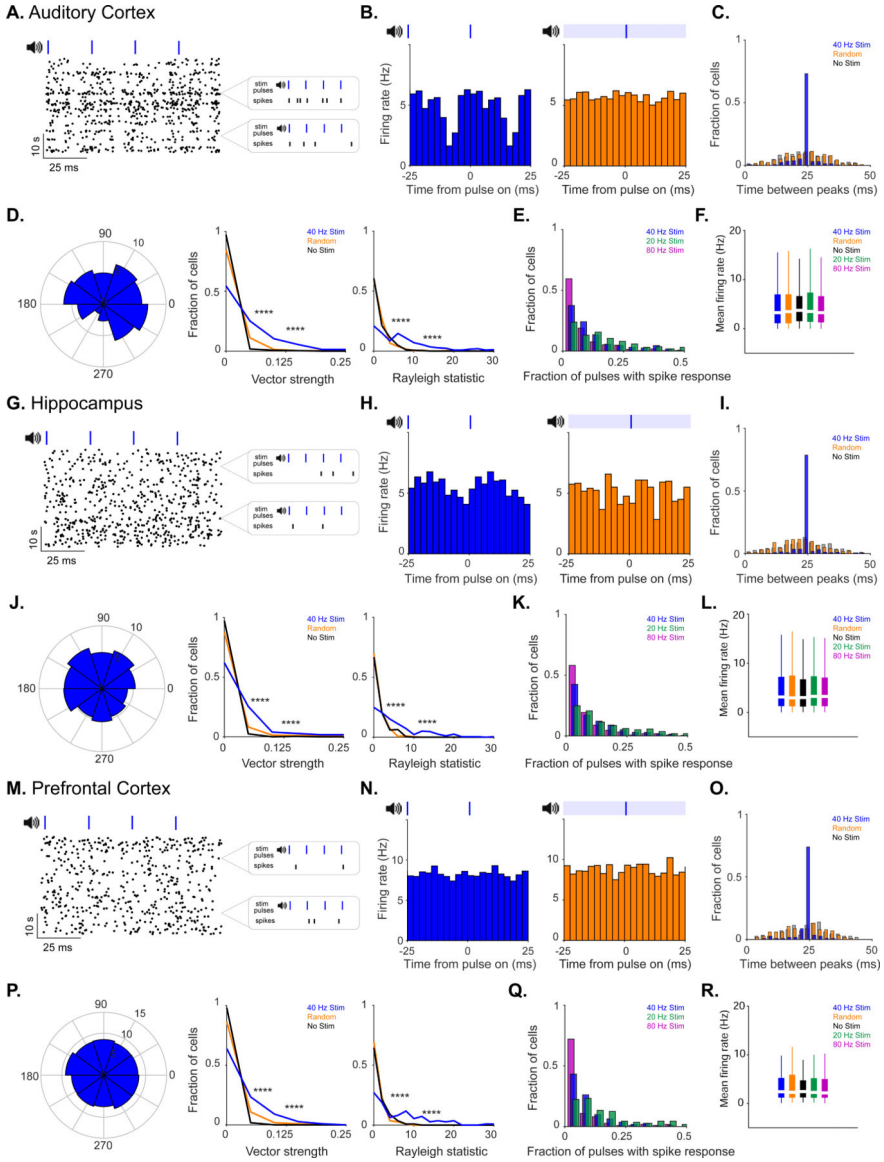

Figure 1. 40 Hz auditory stimulation modulates spiking activity in AC, CA1, and mPFC

A. Example putative single unit spiking response to 40 Hz auditory stimulation with many 10 second stimulation blocks shown wrapped every 100 ms, *left*. Examples of spiking response to four consecutive pulses, *right*.

B. Firing rate modulation of unit shown in **A** during 40 Hz auditory (blue) and random stimulation (orange) in AC. Blue ticks, auditory pulses; light blue bar, randomly distributed pulses.

C. Intervals between peaks in firing rate in AC for no (grey, labeled no stim), random (orange, labeled random), and 40 Hz auditory stimulation (dark blue, labeled 40 Hz stim) conditions for all single units (n = 292 units in 9 recording sessions in 5 mice. Proportion of intervals around inter-stimulus interval: P = 0 40 Hz vs. No stim, P = 0 40 Hz vs. Random; z-Test for two proportions. For all statistics reported, results are significant after controlling for multiple comparisons using the Bonferroni correction unless otherwise stated).

D. Example polar plot of firing rate modulation relative to stimulus onset during 40 Hz auditory stimulation (*left,* stimulus onset at 0), vector strengths of single unit firing rate modulation during 40 Hz auditory, random, and no stimulation (*center,* ****P<0.00005 40 Hz vs. No Stim, 40 Hz vs. Random; Kolmogorov-Smirnov test; 9 units had 40 Hz stim VS values greater than 0.25; 6 units had random stim VS values greater than 0.25), and Rayleigh statistic values of single unit firing rate modulation (*right*, ****P<0.00005 40 Hz vs. No Stim, 40 Hz vs. Random; Kolmogorov-Smirnov test; 40 units had 40 Hz stim RS values greater than 30; 2 units had random stim RS values greater than 30).

E. Fraction of pulses with spiking response from single units in AC for 20 Hz, 40 Hz, and 80 Hz auditory stimulation.

F. Mean firing rates between stimulation conditions in AC.

G. Same as **A** for CA1.

H. Same as **B** for CA1.

I. Same as **C** for CA1 (n = 338 units in 10 recording sessions in 5 mice. P = 0 40 Hz vs. No stim, P = 0 40 Hz vs. Random; z-Test for two proportions).

J. Same as **D** for CA1 (*center,* ****P<0.00005 40 Hz vs. No Stim, 40 Hz vs. Random; Kolmogorov-Smirnov test; 11 units and 2 units had VS values > 0.25 during 40 Hz or random, respectively; right, ****P<0.00005 40 Hz vs. No Stim, 40 Hz vs. Random; Kolmogorov-Smirnov test; 7 units had 40 Hz stim RS values > 30).

K. Same as **E** for CA1.

L. Same as **F** for CA1.

M. Same as **A** for mPFC.

N. Same as **B** for mPFC.

O. Same as **C** for mPFC (n = 115 units in 7 recording sessions in 4 mice. P = 0 40 Hz vs. No stim, P = 0 40 Hz vs. Random; z-Test for two proportions).

P. Same as **D** for mPFC (*center,* ****P<0.00005 40 Hz vs. No Stim, 40 Hz vs. Random; Kolmogorov-Smirnov test; *right*, ****P<0.00005 40 Hz vs. No Stim, 40 Hz vs. Random; Kolmogorov-Smirnov test; 2 units had 40 Hz stim RS values > 30).

Q. Same as **E** for mPFC.

R. Same as **F** for mPFC.

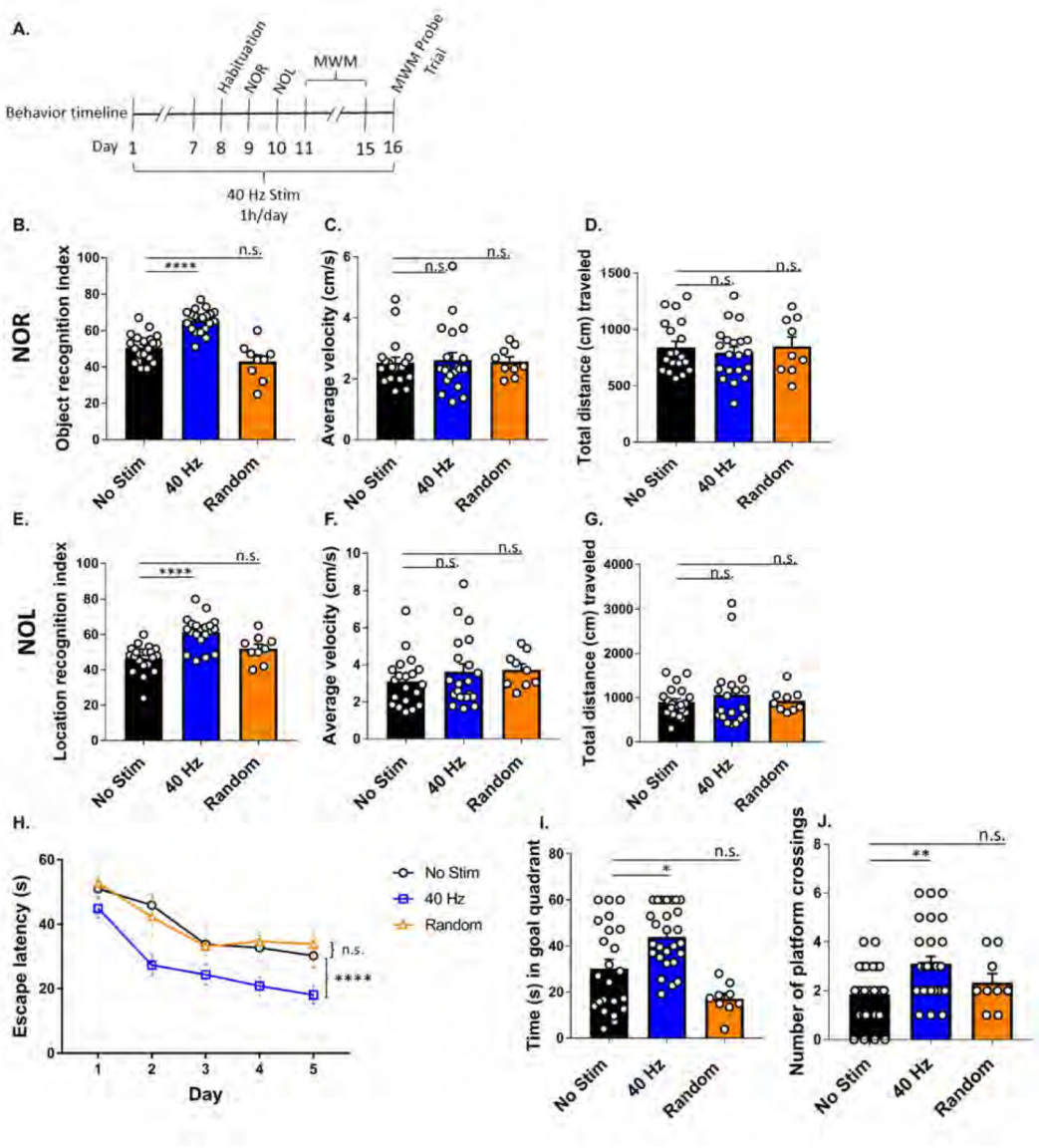

Figure 2. Auditory GENUS improves recognition and spatial memory tasks in 5XFAD mice

A. Timeline of behavior experiments.

B. Recognition index of novel object recognition (NOR) test (n=20 mice no stim [black], n=20 mice 40 Hz [blue], n=9 random frequency [orange], ****P<0.0001, Kruskal-Wallis (KW) test with Dunn's multiple comparison test).

C. Average velocity (cm/s) during novel object recognition test (n=20 mice no stim, n=20 mice 40 Hz, n=9 random frequency, KW-test with Dunn's multiple comparison test).

D. Total distance (cm) traveled during novel object recognition test (n=20 mice no stim, n=20 mice 40 Hz, n=9 random frequency, KW-test with Dunn's multiple comparison test).

E. Recognition index of novel object location (NOL) test of 5XFAD auditory GENUS mice (n=20 mice no stim, n=20 mice 40 Hz, n=9 random frequency, ****P<0.0001, KW-test with Dunn's multiple comparison test).

F. Average velocity (cm/s) during novel object location test (n=20 mice no stim, n=20 mice 40 Hz, n=9 random frequency, KW-test with Dunn's multiple comparison test).
G. Total distance (cm) traveled during novel object location test (n=20 mice no stim, n=20 mice 40 Hz, n=9 random frequency, KW-test with Dunn's multiple comparison test).
H. Escape latencies (s) of 5XFAD mice in the Morris Water Maze (n=25 mice no stim, n=28 mice 40 Hz, n= 9 random frequency, ****P<0.0001, 2-way ANOVA with Tukey's multiple comparison test).
I. Time (s) spent swimming in the goal quadrant during the probe trial (n=25 mice no stim, n=28 mice 40 Hz, n= 9 random frequency, *P<0.05, KW-test with Dunn's multiple comparison test).
J. Number of platform crossings during probe trial (n=25 mice no stim, n=28 mice 40 Hz, n= 9 random frequency, **P<0.01, KW-test with Dunn's multiple comparison test). Circles indicate 'n', mean +/− s.e.m. in bar graphs unless otherwise noted, n.s. = not significant.

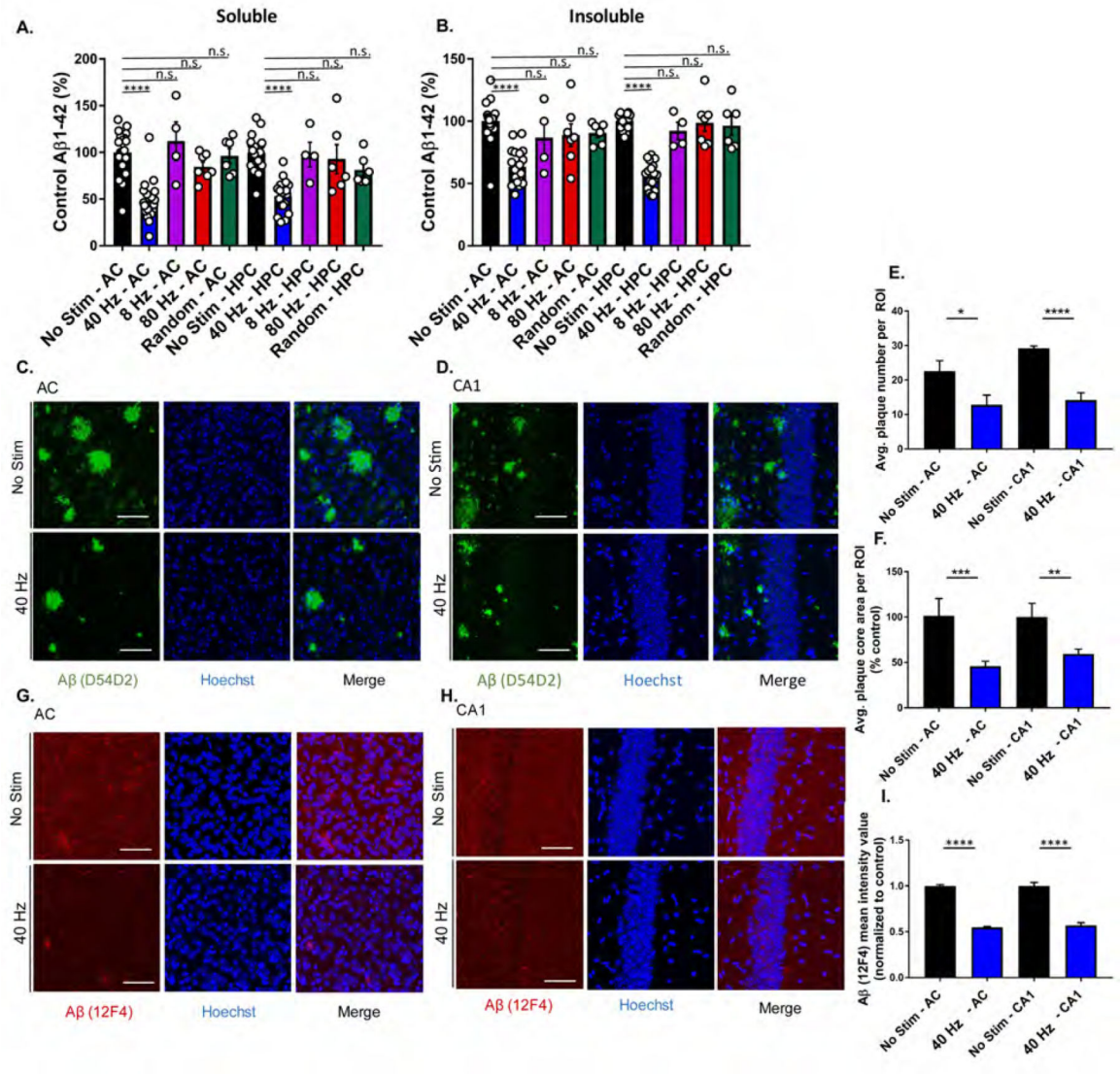

Figure 3. Auditory GENUS reduces amyloid load in AC and HPC in 5XFAD mice

A. Relative soluble $A\beta_{1-42}$ levels in AC and HPC in 6-month-old 5XFAD mice following 40 Hz, 8 Hz, 80 Hz, or random auditory stimulation for 1 hr/day for 7 days (1-week), normalized to non-stimulation control (n=19 mice no stim, n=19 mice 40 Hz, n=4 mice 8 Hz, n=7 80 Hz, n=6 random frequency, ****P<0.0001, KW-test with Dunn's multiple comparison test).

B. As in **A** for insoluble $A\beta_{1-42}$.

C. Immunohistochemistry with anti-Aβ (D54D2, green) antibody in 6-month-old AC of 5XFAD mice after auditory GENUS or no stimulation, for 1 week (n=7 mice/group, scale bar, 50 μm).

D. As in **C** for CA1.

E. Average number of Aβ-positive plaques in AC and CA1 (n=7 mice/group, *P<0.05, ****P<0.0001; unpaired Mann-Whitney Test).

F. Average area of Aβ-positive plaques in AC and CA1 (n=7 mice/group, **P<0.01, ***P<0.001; unpaired Mann-Whitney Test).

G. Immunohistochemistry with anti-Aβ (12F4, red) antibody in 6-month-old AC of 5XFAD mice after auditory GENUS or no stimulation, for 1 week (Inset, 20x, scale bar, 50 μm).

H. As in **G** for CA1.

I. Aβ (12F4) mean intensity value (12F4 antibody) normalized to non-stimulated controls (n=7 mice/ group, ****P<0.0001, unpaired Mann-Whitney Test). Circles indicate 'n', mean +/− s.e.m. in bar graphs unless otherwise noted, n.s. = not significant.

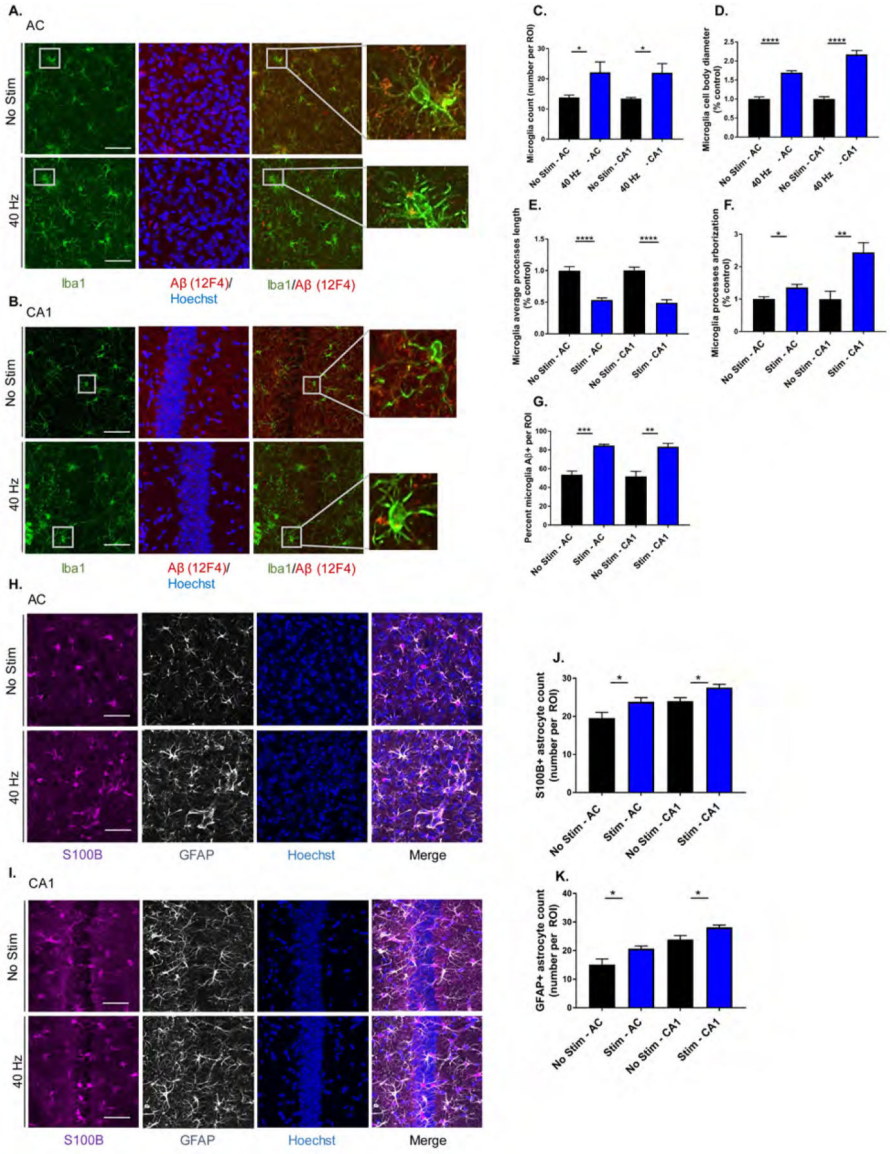

Figure 4. Auditory GENUS induces glial response in AC and CA1 in 5XFAD mice

A. Immunohistochemistry with anti-Iba1 (019–19741, green) and anti-Aβ (12F4, red) antibodies in AC of 5XFAD mice after 7 days of 1 hr/day (1-week) no stimulation or auditory GENUS (n=8 mice/ group, scale bar, 50 μm).

B. As in **A** for CA1

C. Number of Iba1-positive microglia in AC and CA1 (n=8 mice/group, *P<0.05; unpaired Mann-Whitney (MW) Test).

D. Diameter of Iba1-positive microglia cell bodies in AC and CA1 normalized to non-stimulated controls (n=8 mice/group, ****P<0.0001; unpaired MW-Test).

E. Average length of Iba1-positive microglia primary processes in AC and CA1 normalized to non-stimulated controls (n=8 mice/group, ****P<0.0001; unpaired MW-Test).

F. Average processes arborization of Iba1-positive microglia in AC and CA1 normalized to non-stimulated controls (n=8 mice/ group, *P<0.05, **P<0.01; unpaired MW-Test).

G. Percentage of Iba1-positive microglia cell bodies that are also Aβ-positive in AC and CA1 (n=8 mice/group, **P<0.01, ***P<0.001; unpaired MW-Test).

H. Immunohistochemistry with anti-S100B (ab868, purple) and anti-GFAP (ab4674, grey) antibodies in AC of 5XFAD mice after 1-week no stimulation or auditory GENUS (n=8 per group, scale bar, 50 μm).

I. As in **H** for CA1.

J. Number of S100B-positive astrocytes in AC and CA1 (n=8 mice/group, *P<0.05; unpaired MW-Test).

K. As in **J** for GFAP-positive astrocytes. Circles indicate ‘n’, mean +/− s.e.m. in bar graphs unless otherwise noted, n.s. = not significant.

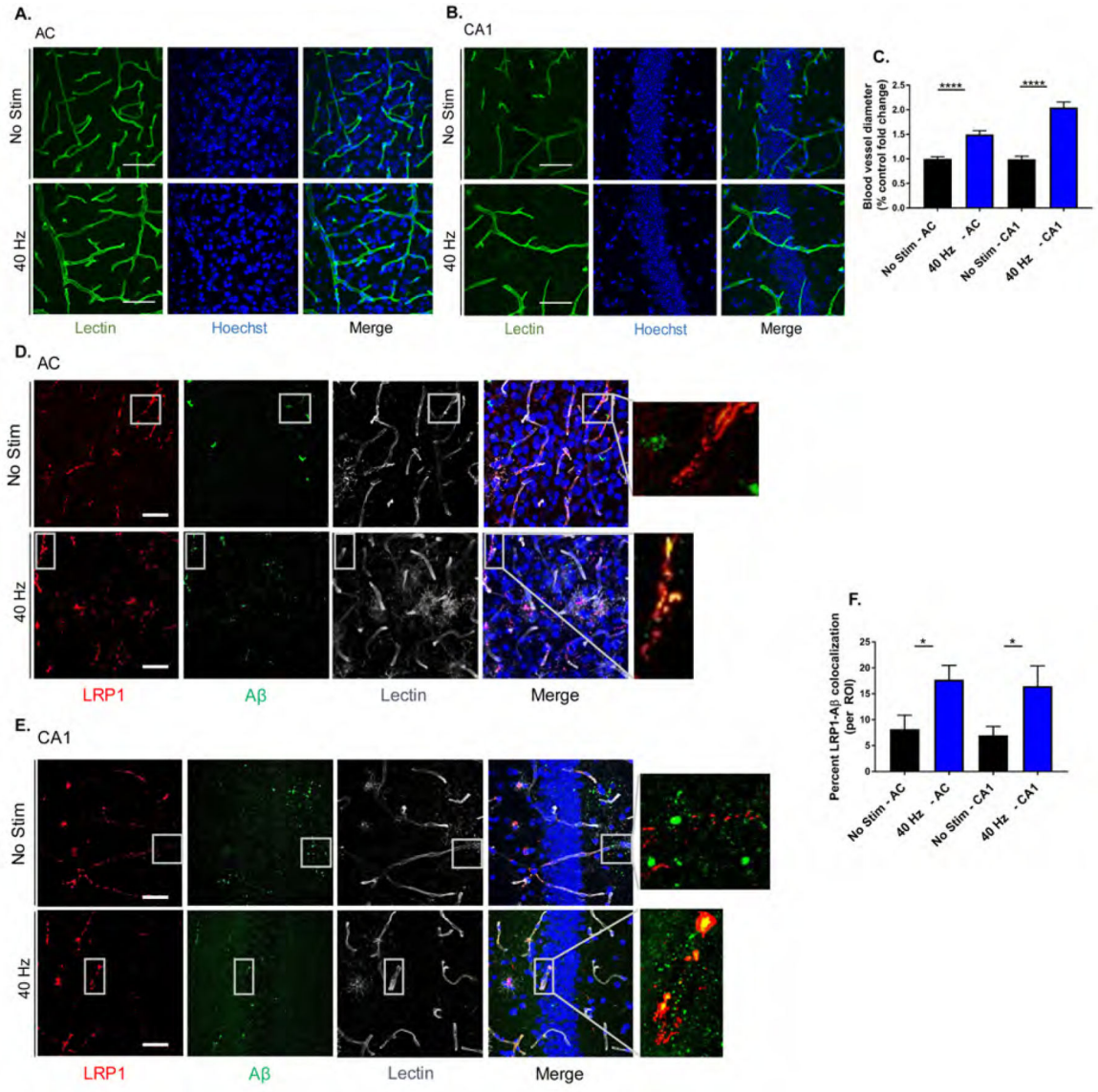

Figure 5. Auditory GENUS increases amyloid-vasculature associations.

A. Immunohistochemistry with lectin stain (DL-1174, green) in AC of 6-month-old 5XFAD mice after 7 days of 1 hr/day (1-week) no stimulation or auditory GENUS (scale bar, 50 μm).

B. As in **A** for CA1.

C. Percent fold change in blood vessel diameter in AC and CA1 of 6-month-old 5XFAD mice after 1-week no stimulation or auditory GENUS, normalized to no stimulation control (n=7 mice/group, ****P<0.0001; unpaired Mann-Whitney (MW) Test).

D. Immunohistochemistry with anti-LRP1 (28320, red), anti-Aβ (AB9234, green), and lectin stain (DL-1174, gray) antibodies in AC of 6-month-old 5XFAD mice after 1-week no stimulation or auditory GENUS (n=8 mice/group, scale bar, 50 μm).

E. As in **D** for CA1.

F. Percentage of Aβ-LRP1 co-localization in AC and CA1 of 5XFAD mice after 1-week no stimulation or auditory GENUS (n=8 mice/group, *P<0.05; unpaired MW-test). Circles indicate ‘n’, mean +/−s.e.m. in bar graphs unless otherwise noted, n.s. = not significant.

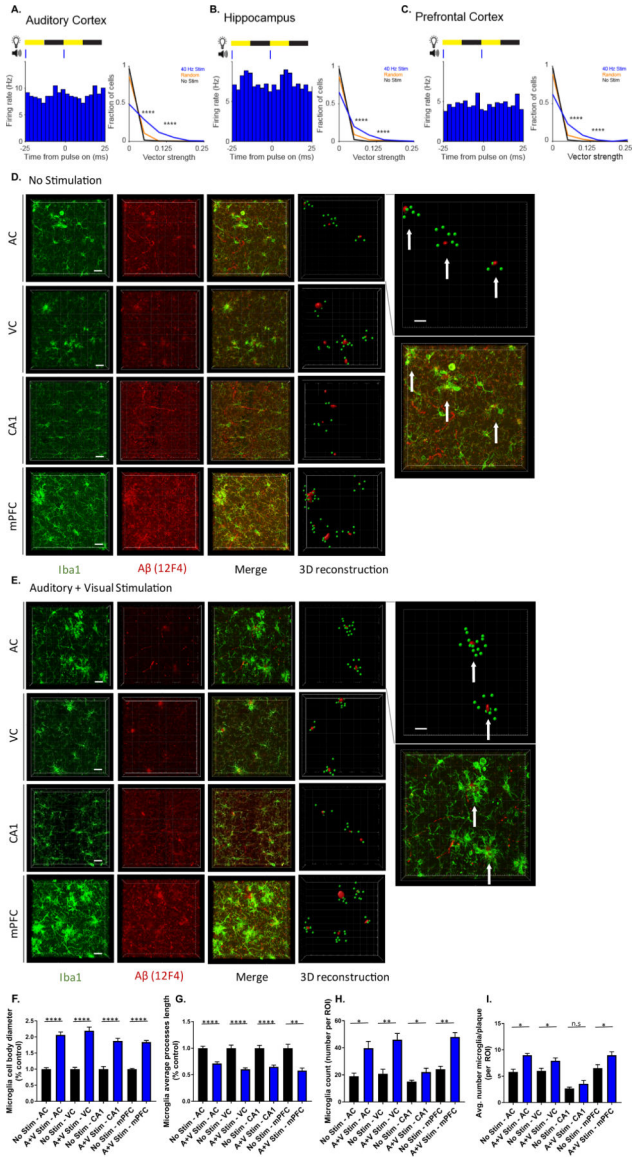

Figure 6. Combined auditory and visual GENUS induces a clustering phenotype response by microglia

A. Firing rate modulation of a single unit during 40 Hz audio-visual stimulation (*left).* Vector strength of responses to 40 Hz A+V stimulation, random A+V stimulation, and no stimulation periods (*right,* ****P<0.00005 40 Hz vs. No Stim, 40 Hz vs. Random; Kolmogorov-Smirnov test; 9 units had 40 Hz stim VS values greater than 0.25; 3 units had random stim VS values greater than 0.25. In all statistical tests for panels A-C, results are significant after controlling for multiple comparisons using the Bonferroni correction unless otherwise stated).

B. Same as **A** for CA1 (*right,* ****P<0.00005 40 Hz vs. No Stim, 40 Hz vs. Random; Kolmogorov-Smirnov test; 8 units and 3 units had VS values > 0.25 for 40 Hz or random stim, respectively).

C. Same as **A** for mPFC (*right*, ****P<0.00005 40 Hz vs. No Stim, 40 Hz vs. Random; Kolmogorov-Smirnov test; 5 units had 40 Hz stim VS values > 0.25).

D. Immunohistochemistry and 3D reconstruction using IMARIS (Methods) of anti-Iba1 (019–19741, green) and anti-Aβ (12F4, red) antibodies in AC, VC, CA1, and mPFC of 6-month-old 5XFAD mice after 7 days of 1 hr/day (1-week) of no stimulation (n=6 mice/group, *top* inset: example of using IMARIS to quantify the number of microglia surrounding a 25 μm radius around amyloid plaques. Plaques as red dots, microglia as green dots, and white arrows point to clusters. *Bottom* inset: enlarged merged image from AC. Scale bar, 20 μm).

E. As in **D** for combined GENUS.

F. Average microglia cell body diameter in AC, VC, CA1, and mPFC of 6-month-old 5XFAD mice after 1-week no stimulation or combined GENUS, normalized to no stimulation control (n=6 mice no stim, n=7 mice combined GENUS, ****P<0.0001; unpaired Mann-Whitney (MW) test).

G. Average microglia process length in AC, VC, CA1, and mPFC of 6-month-old 5XFAD mice after 1-week no stimulation or combined GENUS, normalized to no stimulation control (n=6 mice no stim, n=7 mice combined GENUS, **P<0.01, ****P<0.0001; unpaired MW-test).

H. Microglia count per region of interest in AC, VC, CA1, and mPFC of 6-month-old 5XFAD mice after 1-week no stimulation or combined GENUS (n=6 mice no stim, n=7 mice combined GENUS, *P<0.05, **P<0.01, unpaired MW-Test).

I. Average number of microglia surrounding 25 μm radium of a plaque in AC, VC, CA1, and mPFC following no stimulation or combined GENUS (n=6 mice/group, *P<0.05; unpaired MW-Test). Circles indicate ‘n’, mean +/− s.e.m. in bar graphs unless otherwise noted, n.s. = not significant.

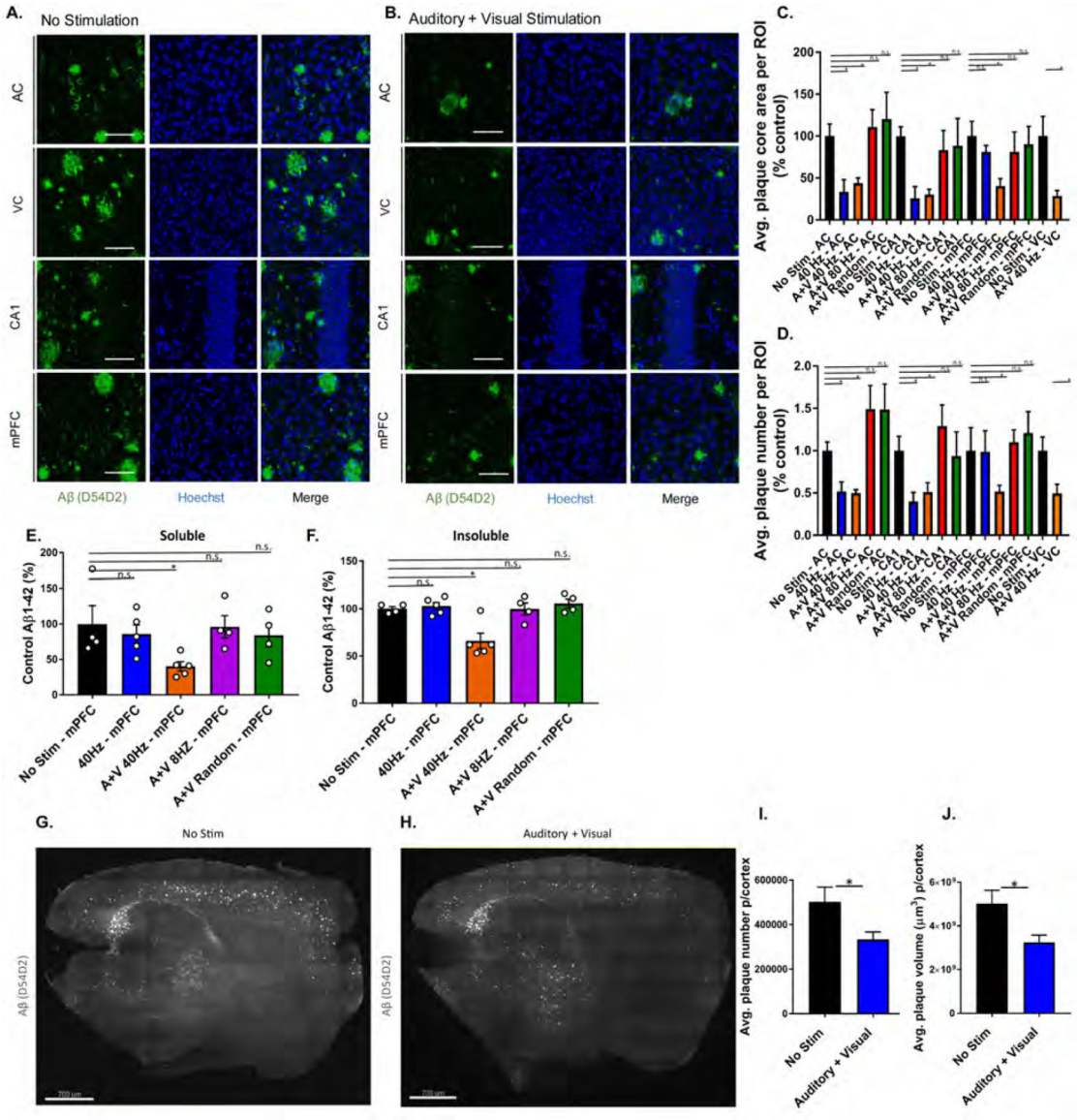

Figure 7. Combined auditory and visual GENUS reduces amyloid load in the mPFC and neocortex

A. Immunohistochemistry of anti-Aβ plaques (D54D2, green) antibodies in AC, VC, CA1, and mPFC of 6-month-old 5XFAD mice after 7 days of 1 hr/day (1-week) no stimulation (40x objective, scale bar, 50 μm).

B. As in **A** for combined GENUS.

C. Average plaque core area in AC, CA1, mPFC, and VC in 6-month old 5XFAD mice following 1-week no stimulation, 40 Hz auditory stimulation, combined GENUS, combined 80 Hz, and combined random frequency stimulation, normalized to no stimulation control (n=12 mice/group, *P<0.05, Kruskal-Wallis (KW) test with Dunn's multiple comparison test)

D. Average plaque number in AC, CA1, mPFC, and VC in 6-month old 5XFAD mice following 1-week no stimulation, 40 Hz auditory stimulation, combined GENUS, combined

80 Hz, and combined random frequency stimulation, normalized to no stimulation control (n=12 mice/group, *P<0.05, KW-test with Dunn's multiple comparison test).

E. Relative soluble $A\beta_{1-42}$ levels in mPFC of 6-month-old 5XFAD mice following 1-week 40 Hz auditory stimulation, combined GENUS, combined 8 Hz, or combined random frequency stimulation, normalized to non-stimulation control (n=4–5 mice per group, *P<0.05, KW-test with Dunn's multiple comparison test).

F. As in **E** for insoluble $A\beta_{1-42}$ (*P<0.05).

G. Immunohistochemistry of SHIELD treated whole brain (sagittal plane of 25 μm section of brain) of anti-Aβ plaques (D54D2, white) antibodies of 6-month-old 5XFAD mice after 1-week no stimulation (light-sheet microscope, scale bar, 700 μm).

H. As in **G** for combined GENUS.

I. Average cortical plaque number following no stimulation or combined GENUS (n=6 mice/group, *P<0.05; unpaired MW-Test).

G. Average cortical plaque volume (μm^3) following combined GENUS (n=6 mice/group, *P<0.05; unpaired MW-Test). Circles indicate 'n', mean +/− s.e.m. in bar graphs unless otherwise noted, n.s. = not significant.